Control of Chemical Dynamics by Lasers: Theoretical Considerations

ARTICLE *in* THE JOURNAL OF PHYSICAL CHEMISTRY A · JUNE 2010

Impact Factor: 2.69 · DOI: 10.1021/jp911579h · Source: PubMed

4 AUTHORS, INCLUDING:

Shinkoh Nanbu
Sophia University
107 PUBLICATIONS **895** CITATIONS
SEE PROFILE

Yoshiaki Teranishi
National Chiao Tung University
43 PUBLICATIONS **371** CITATIONS
SEE PROFILE

Hiroki Nakamura
National Chiao Tung University
238 PUBLICATIONS **4,088** CITATIONS
SEE PROFILE

Control of Chemical Dynamics by Lasers: Theoretical Considerations

Alexey Kondorskiy,[†] Shinkoh Nanbu,[‡] Yoshiaki Teranishi,[§] and Hiroki Nakamura*

Institute for Molecular Science, National Institutes of Natural Sciences, Myodaiji, Okazaki 444-8585, Japan

Received: December 7, 2009; Revised Manuscript Received: February 25, 2010

Theoretical ideas are proposed for laser control of chemical dynamics. There are the following three elementary processes in chemical dynamics: (i) motion of the wave packet on a single adiabatic potential energy surface, (ii) excitation/de-excitation or pump/dump of wave packet, and (iii) nonadiabatic transitions at conical intersections of potential energy surfaces. A variety of chemical dynamics can be controlled, if we can control these three elementary processes as we desire. For (i) we have formulated the semiclassical guided optimal control theory, which can be applied to multidimensional real systems. The quadratic or periodic frequency chirping method can achieve process (ii) with high efficiency close to 100%. Concerning process (iii) mentioned above, the directed momentum method, in which a predetermined momentum vector is given to the initial wave packet, makes it possible to enhance the desired transitions at conical intersections. In addition to these three processes, the intriguing phenomenon of complete reflection in the nonadiabatic-tunneling-type of potential curve crossing can also be used to control a certain class of chemical dynamics. The basic ideas and theoretical formulations are provided for the above-mentioned processes. To demonstrate the effectiveness of these controlling methods, numerical examples are shown by taking the following processes: (a) vibrational photoisomerization of HCN, (b) selective and complete excitation of the fine structure levels of K and Cs atoms, (c) photoconversion of cyclohexadiene to hexatriene, and (d) photodissociation of OHCl to O + HCl.

I. Introduction

Recent progress of chemical dynamics theory and laser technology is remarkable, and now we can think of controlling various elementary processes of chemical dynamics.[1−11] Control of chemical reactions is not just a simple unrealizable dream anymore. Various ideas have been proposed so far such as the coherent control, the adiabatic rapid passage, the quadratic chirping, utilization of complete reflection phenomenon, and the optimal control theory, as explained in the reviews and books.[3−11] Recently, significant progress has been made in experimental realization of the adaptive closed-loop control (see ref 12). Several successful experiments demonstrate the ability of the technique to control observables (see refs 13 and 14). However, from our viewpoint these are not necessarily good enough to gain physical insights and to formulate a general concept.

In this Feature Article we present some of our recent theoretical achievements on controlling chemical dynamics based on our own ideas and theories in comparison with the others. We emphasize the significance of nonadiabatic chemical dynamics, in general, and also important roles of nonadiabatic transitions in laser-induced chemical dynamics (see Chapter 13 of ref 5). Whenever the nonadiabatic transitions due to potential curve or surface crossings have to be treated, the Zhu−Nakamura theory can be usefully utilized.[5,10] Comprehending and clarifying the physical and chemical mechanisms are another important factor we have to consider, and the theory is helpful for that. There are three basic elements in chemical dynamics: (i) motion of quantum wave packet on an adiabatic potential energy surface including its rotational motion, (ii) excitation and de-excitation of energy levels, or pump and dump of the wave packet, and (iii) transitions at conical intersections of potential energy surfaces. If we could control these processes as we desire, control of various chemical dynamics would be possible. For the control of wave packet motion, the idea of so-called optimal control theory is most suitable to design an appropriate laser field.[4,15−21] The selective and localized bond stretching has been conventionally used in photodissociation (see, for instance, ref 22). The optimal control theory is more versatile, and we have formulated its semiclassical version so that we can deal with multidimensional systems by guiding the initial wave packet properly.[23,24] Highly efficient excitation/de-excitation of energy levels and pump/dump of the wave packet can be achieved by controlling the laser-induced nonadiabatic transition among the so-called dressed states with use of the quadratic chirping method.[25,43] Dressed states mean the states shifted up or down by the amount of photon energy, $\hbar\omega$. Although the linear chirping has been proposed and used in various processes,[4,26−28] our idea of periodic chirping is its generalization and is more versatile. As for controlling the transitions at conical intersections, we also have to think about controlling the wave packet motion, since potential energy surface topography of conical intersection and the nonadiabatic coupling there are determined by Nature and we cannot modify them easily by lasers. Instead, we can control the nonadiabatic transitions there by giving an appropriately directed momentum to the wave packet (directed momentum method).[29,30] It is true that we can change the geometry of potential energy surfaces by using a very strong laser, but it causes many undesirable multiphoton processes and is not appropriate. Thus the laser intensity should probably be lower than ∼10 TWatts/cm^2. The second requirement we have to consider is the time duration to complete the appropriate

[†] Present address: P. N. Lebedev Physical Institute, Leninsky pr., 53, Moskow 119991, and Moscow Institute of Physics and Technology, Institutsky per., 9, Dolgoprudny, Moscow Region 141700, Russia.

[‡] Present address: Departnment of Materials and Life Sciences, Faculty of Science and Technology, Sophia University, 7-1 Kioi-cho, Chiyoda-ku, Tokyo 102-8554, Japan.

[§] Present address: Department of Applied Chemistry, National Chiao Tung University, 1001 Ta Hsueh Rd., Hsinchu 30010, Taiwan.

10.1021/jp911579h
Published on Web 05/10/2010

Alexey D. Kondorskiy received his M.S. degree in physics from the Moscow Institute of Physics and Technology (State University) in 1998 and his Ph.D. in 2001 from the same university. In 2001−2006 he worked at the Institute for Molecular Science in Japan. Since 2006 he has been working at the P. N. Lebedev Physical Institute of the Russian Academy of Science, where he is now a senior researcher. His research interests are theoretical studies of optical control, semiclassical theory of molecular dynamics, optics, and spectroscopy of semiconductor nanoparticles.

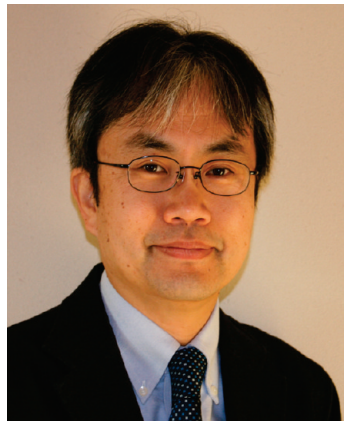

Shinkoh Nanbu was born in Miyagi, Japan, in 1964. He completed his doctorate in Chemistry at Keio University, Japan, in 1994. From 1991 to 1992, he was a JSPS doctoral fellow at Keio University. In 1992, he became an Assistant Professor at the Computer Centre of the Institute for Molecular Science. He moved to the Computer Centre of Kyushu University in 2005. Since 2009, he has been a Professor in the Faculty of Science and Technology for Sophia University, Tokyo, Japan. His current interests include photochemistry, nonadiabatic phenomena, and isotope fractionation in atmospheric chemistry.

process. This is especially important when any competing processes such as relaxation processes exist. It is required to finish the desirable control process as quickly as possible. The third requirement to be satisfied is that the laser pulse shape should be as simple as possible to make actual pulse shaping feasible. In addition to the above-mentioned three elementary processes (i)−(iii), it is also worthwhile to think about applications of the *complete reflection* phenomenon that occurs in the nonadiabatic tunneling-type potential curve crossing in which two diabatic potential curves cross with the opposite signs of slopes [Chapter 11 of ref 5].[10,31−33] This intriguing phenomenon occurs at certain discrete energies higher than the bottom of the upper adiabatic potential. This phenomenon cannot be complete in multidimensional systems, but it may survive to some extent and can be used to control some chemical dynamics and also to manifest some molecular functions [Chapters 12 and 13 of ref 5].[34]

This paper is organized as follows: In section II the ideas of the above-mentioned four controlling schemes will be qualitatively explained. Section III presents the semiclassical theories

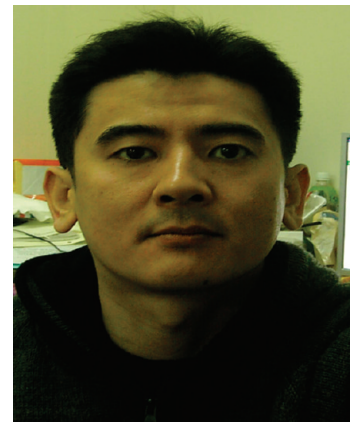

Yoshiaki Teranishi is a research Assistant Professor of the Department of Applied Chemistry at National Chiao-Tung University. He received his BA in liberal arts and M.Sc. from International Christian University. He earned his Ph.D from the Graduate University for Advanced Studies. His research interests are intense field science and chemical reaction dynamics.

Hiroki Nakamura is Director General of IMS and Executive Director and Vice President of NINS (National Institutes of Natural Sciences). He received his Ph.D. from The University of Tokyo. His scientific interests are the theory of chemical dynamics, semiclassical theory, and nonadiabatic transition.

for the guided optimal control and the quadratic frequency chirping. Corresponding numerical demonstrations of these control schemes will be described in section IV, taking real atoms and molecules as examples. Section V concludes the discussions and presents future perspectives.

II. Basic Ideas

1. Control of Wave Packet Motion on Adiabatic Potential Energy Surface. The most basic element of chemical dynamics to be controlled is the relative motion of reactant molecules. Theoretically, this means to control the motion of a quantum wave packet on a given adiabatic potential energy surface. To design a laser field that can lead the initial wave packet to a given target state with high efficiency, the so-called optimal control theory would be most appropriate. Various versions of the theory have been proposed so far (see, for instance, ref 4). There are two problems to be solved, however. Since the phase of laser field plays significant roles in controlling, the classical mechanical version of the theory cannot be used.[35,36] Since it is desirable to treat realistic multidimensional systems, the quantum mechanical versions are not very appropriate, unfortunately, because they are still numerically too heavy and cannot treat systems of higher than three dimensions. We have formulated a semiclassical version with use of the Herman−Kluk-type frozen Gaussian wave packet propagation method[37] based on

the quantum conjugate gradient search method.[19] Another problem we have to overcome is the inefficiency of any method originating from the small overlap between the initial and target states in multidimensional space. The basic idea of optimal control theory is naturally to maximize the overlap between the trial and target states by iteratively solving the time-dependent Schrödinger equations. This procedure becomes very time-consuming and inefficient, when the overlap between the initial and target states is small. To overcome this difficulty, it is natural to guide the initial wave packet toward the target by setting appropriate intermediate target states.[23,24,38,39] The intermediate target states are not necessarily accurate but can be appropriately given. The actual formulation and numerical examples are given in sections III.1 and IV.1, respectively. In principle, this method can, of course, be employed to enhance electronic excitation/de-excitation or pump/dump of the wave packet and also to control the nonadiabatic transitions at conical intersections. For these elementary processes, however, we propose more direct and physical ideas. These ideas are discussed in the following two subsections. The clear physical ideas are helpful to simplify the required laser pulses.

2. Giving Pre-Determined Directed Momentum to Wave Packet. Nonadiabatic chemical dynamics holds a significant position in chemistry,[5,10] and conical intersections play crucial roles in the dynamics.[40] The concept of conical intersection is purely theoretical but is crucial for understanding and interpreting experimental observations, as is well-known. Conical intersections in molecules are naturally given; i.e., the topography of the potential energy surfaces and the nonadiabatic coupling between the corresponding two surfaces are determined by Nature and we cannot change them. It is true that the potential energy surfaces are modified and the additional coupling between the two surfaces is induced by a strong laser. However, such a strong laser induces many undesirable multiphoton processes and is not convenient for controlling the transition at the conical intersection. Instead, we can give an appropriate momentum vector to the wave packet so that the nonadiabatic transition at the conical intersection occurs in a favorable way. This is called the *directed momentum method*. One numerical demonstration of enhancing the photoconversion efficiency was carried out in the photochromic cyclohexadiene (CHD)/hexatriene (HT) system by giving an appropriate directed momentum to the initial wave packet.[30] Since giving an appropriate momentum to the wave packet is just an example of controlling the wave packet motion, the optimal laser can be designed by using the semiclassical guided optimal control theory. This directed momentum method is quite general and is not restricted to the transition at conical intersections but is applicable to many other processes. Controlling other types of nonadiabatic transition and branching of molecular photodissociation would be good examples. Numerical examples are given in sections IV.2 and IV.4 for the above-mentioned CHD/HT system and photodissociation of OHCl, respectively. A very rough consideration about the appropriate laser for directing the momentum may be made as follows. The momentum given to the wave packet by laser is expressed as follows[41]

$$P = -i\hbar\langle\Psi_0|\hat{U}^{\dagger}(t)\,\nabla_{\mathbf{r}}\hat{U}(t)|\Psi_0\rangle = -i\hbar\langle\Psi_0|\hat{U}^{\dagger}(t)\,(\nabla_{\mathbf{r}}\hat{\Omega}(t))\,\hat{U}(t)|\Psi_0\rangle \quad (1)$$

with

$$\hat{\Omega}(t) = \int_0^t \hat{H}_I(\tau)\,d\tau + \frac{1}{2}\int_0^t d\tau \int_0^\tau d\tau' \,[\hat{H}_I(\tau) + \hat{H}_0(\tau), \hat{H}_I(\tau') + \hat{H}_0(\tau')] + \ldots \quad (2)$$

Here $\mathbf{r}$, $|\Psi_0\rangle$, $\hat{U}(t) = \exp[\hat{\Omega}(t)]$, $\hat{H}_0$, and $[\cdots, \cdots]$ are the molecular internal coordinate, the initial state, the evolution operator of the system, Hamiltonian of the molecule, and the commutator. The laser−molecule interaction is $H_I = -\vec{\mu}(\mathbf{r})\cdot\mathbf{E}(t)$, where $\vec{\mu}(\mathbf{r})$ and $\mathbf{E}(t)$ are the 3-D dipole moment vector and laser field vector, respectively. Since $\nabla_{\mathbf{r}}\hat{\Omega}(t)$ contains $\nabla_{\mathbf{r}}\vec{\mu}(\mathbf{r})\cdot\mathbf{E}(t)$, it is expected that the appropriate laser field is parallel to the derivative of the dipole moment vector in the direction of the desirable momentum. In the case of a polyatomic molecule, the number of molecular internal coordinates is larger than the degrees of freedom of the laser field, but the important geometry of conical intersection is usually determined locally by a few molecular internal coordinates and it is expected to be feasible to adjust the laser field to the appropriate direction, as mentioned above. This very rough idea may be used as the zero-th order approximation in the iteration procedure to determine the optimal field. Actually, this is found to be useful in the numerical demonstrations given in sections IV.2 and IV.4.

3. Efficient Excitation/De-Excitation by Inducing Nonadiabatic Transition. Let us next consider control of excitation/de-excitation of energy levels, or pump/dump of the wave packet,[17] with high efficiency. In the ordinary excitation/de-excitation process, the perturbation theory is good enough to estimate the corresponding probability. In the case of a strong laser field, on the other hand, the dressed state picture is useful, as explained above, and the excitation/de-excitation can be considered as a time-dependent nonadiabatic transition between the dressed states. Since the coupling between the states is the laser−molecule dipole interaction, we can control the transition by appropriately manipulating laser parameters. We have proposed the quadratic chirping, or more generally, the periodic chirping (see Chapter 13 of ref 5 and also refs 10 and 25) in which the laser frequency is varied quadratically or periodically as a function of time so that potential energy curve crossings among the dressed states are created twice or more. We can design the laser pulse so that the interference among nonadiabatic transitions at these curve crossings occurs constructively to enhance the efficiency of the final state. In the case of energy levels, this idea can be analytically formulated and the efficiency can be made to be 100%. Numerical calculations have been made so far for the model systems of two to four energy levels, and it was demonstrated that the selective and complete excitation is actually possible (see Chapter 13 of ref 5 and also refs 10 and 42). The idea can further be generalized to the other types of nonadiabatic transitions (see Chapter 13 of ref 5 and also ref 43). In the case of pump or dump of the wave packet, there are two problems and the efficiency cannot be 100%. The wave packet has energy and spatial distribution and also moves on the potential energy surface. We have to design the laser pulse by taking into account the spread and by chirping the frequency as quickly as possible before the wave packet moves away. This can be done, and the efficiency can still be made quite high, if not 100%.[10,44,45] When it comes to resonant excitation, the π-pulse method is well-known. For the transition from one diabatic state to the other, various versions of the adiabatic rapid passage have been proposed such as STIRAP.[4,7,46] In comparison with the present quadratic chirping method, the π-pulse method is simple but it takes time and is somewhat unstable against the pulse shaping. The adiabatic rapid passage is robust, but it requires a strong intensity and long time to

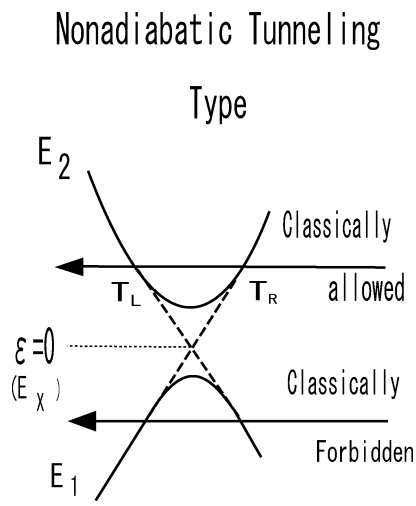

Figure 1. Nonadiabatic-tunneling-type potential curve crossing. $T_{L(R)}$ represents the turning point on the upper adiabatic potential.

achieve the high efficiency.[10,42] The quadratic chirping enables us to achieve the goal quickly, even as shortly as the uncertainty principle allows. Numerical demonstrations of quadratic chirping are presented in section IV.3 for the selective and complete excitation of the fine structures of real atoms K and Cs. The Cs case is a two-photon excitation process.

4. Utilization of the Complete Reflection Phenomenon. In the development of the Zhu−Nakamura theory, it was found that the intriguing phenomenon of *complete reflection* occurs at some discrete energies when the diabatic potentials cross with opposite signs of slopes (see Figure 1).[31−33] This was proved to be quantum mechanically exact in the linear potential model (linear diabatic potentials with constant coupling). The transmission probability from the right side to the left or vice versa is given by (see Chapter 5 of ref 5)

$$P_{12} = \frac{4|\mathrm{Im}\ U|^2}{(|U|^2 - 1)^2 + 4(\mathrm{Im}\ U)^2} \tag{3}$$

where U is the so-called Stokes constant, which is actually a function of effective potential parameters and energy. When $\mathrm{Im}(U) = 0$, which is actually satisfied at certain discrete energies higher than the bottom of the upper adiabatic potential, no transmission occurs; i.e., complete reflection happens. It was proved that this phenomenon also occurs in general curved potentials and the practically useful semiclassical formulas applicable to general curved potentials were derived (see Chapter 5 of ref 5 and also refs 10 and 31). The Zhu−Nakamura theory provides the accurate semiclassical expressions as

$$U = \mathrm{i}(1 - p)^{1/2} \exp[\mathrm{i}\Psi] \tag{4}$$

and

$$P_{12} = \frac{4\cos^2\Psi}{4\cos^2\Psi + p^2/(1 - p)} \tag{5}$$

where p is the nonadiabatic transition probability for one passage of the crossing point and Ψ is the sum of the phase between the two turning points on the upper adiabatic potential and the phase due to the nonadiabatic transition. Thus the complete

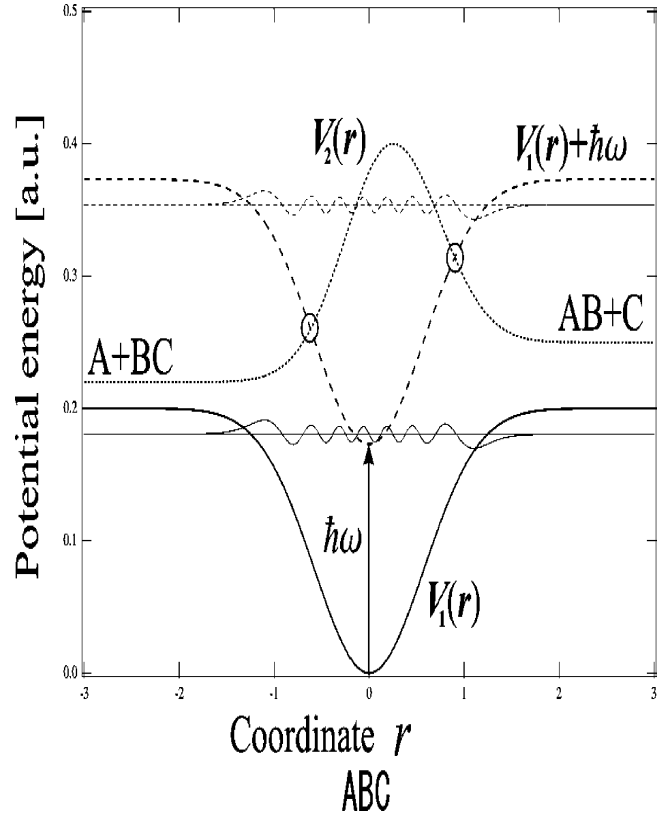

Figure 2. Control of photodissociation with use of the complete reflection phenomenon. $V_{1(2)}(\mathbf{r})$ is the ground (excited) state, $V_1(\mathbf{r}) + \hbar\omega$ is the dressed state, and the two circles represent the laser-induced crossings.

reflection occurs at energies corresponding to $\cos\Psi = 0$, which is the modification of the famous Bohr−Sommerfeld quantization condition. This phenomenon is physically as well as mathematically very unique and is interpreted as follows. Destructive interference occurs for the transmission between the wave trapped by the upper adiabatic potential and the wave transmitting through the potential system without trapping. The uniqueness of this phenomenon stimulates us to think about various applications such as molecular switching, the bound state in the continuum, and control of molecular photodissociation. It is true that this phenomenon is complete only in one-dimension, but some residual effects can be expected to survive in multidimensions. Figure 2 explains the concept of photodissociation control using this phenomenon. The attractive ground state is dressed-up by the CW laser and crosses the repulsive-type excited state at two positions. The complete reflection condition can be created at any one of the crossings by adjusting the laser frequency. If the condition is satisfied at the right side crossing, for instance, then the molecule cannot move out to the right and totally dissociates into the left. It should be noted that vibrational excitation in the initial ground state is required, since enough of the phase is required at the upper adiabatic potential for the condition to be satisfied.

Numerical demonstrations have been already made for various possible applications. If we have a series of nonadiabatic-tunneling-type potential systems, then we can think of molecular switching, since the complete reflection and complete transmission occur at different discrete energies. This possibility has been discussed not only for one-dimensional but also for two-dimensional systems (see Chapter 12 of ref 5 and also refs 47−49). This idea of using complete reflection and transmission leads to an interesting possibility of hydrogen transmission

through five-membered or six-membered carbon rings, which could be related to hydrogen encapsulation by carbon nanomaterials.[34,50] Another possible application is that the system consisting of the same two nonadiabatic-tunneling-type potentials can support *bound states in the continuum* (see Chapter 11 of ref 5 and also refs 48). Very interestingly, this is a real bound sate with infinite lifetime in the continuum. The complete reflection condition can also be realized, when the left side of the lower adiabatic potential is a repulsive wall. This actually represents predissociation of diatomic molecule. The dissociation dip in the IBr molecule is supposed to be due to this phenomenon.[51] In the case of the HI molecule, the photodissociation to H + $I(^2P_{3/2})$ via the $^1\Pi_1$ and $^3\Pi_1$ states can be stopped by this phenomenon, and the dissociation to H + $I^*(^2P_{1/2})$ via the state $^3\Pi_{0+}$ can be made at almost 100% efficiency.[10,52] Multidimensional examples are also demonstrated, taking the two-dimensional models of H_2O and CH_3SH molecules (see Chapter 13 of ref 5 and also ref 53). It should be noted that the phenomenon of complete reflection not only is restricted to the potential system shown in Figure 1 but also can occur in some other cases (see Chapter 11 of ref 5 and also ref 54). We do not go into further details here.

III. Semiclassical Theories

1. Semiclassical Guided Optimal Control Theory.[23,24] Obviously, the goal of the optimal control theory[4] is to design a laser field $\{E_k(t)\}$ such that the wave packet $\phi(t)$ propagated from the initial state $\phi(t = 0) = \Phi_I$ becomes as close as possible to the desired target state Φ_T at time $t = T$. When we employ the simplest form of global optimization procedure with the iterative gradient search method,[19] the correction $\delta E_k(t)$ to the optimal field at each iteration is given by

$$\delta E_k(t) = \hbar^{-1}\langle\Phi_T|\phi(T)\rangle\,\mathrm{Im}[\Theta_k(t)] \tag{6}$$

with the correlation function $\Theta_k(t)$ defined as

$$\Theta_k(t) = \langle\phi(t)|\mu_k(\mathbf{r})|\chi(t)\rangle \tag{7}$$

where $\mu_k(\mathbf{r})$ is the dipole moment with k denoting the polarization vector component.

The wave packets $\phi(t)$ and $\chi(t)$ are propagated forward and backward, respectively, according to the time-dependent Schrödinger equation,

$$\left[\mathrm{i}\hbar\frac{\partial}{\partial t} + \sum_{j=0}^{N}\frac{\hbar^2}{2m_j}\frac{\partial^2}{\partial r_j^2} - V(\mathbf{r}) + \sum_{k=1}^{3}\mu_k(\mathbf{r})\,E_k(t)\right]\psi(t) = 0 \tag{8}$$

with $\psi(t = 0) = \Phi_I$ in the case of $\psi = \phi$ and $\psi(t = T) = \Phi_T$ in the case of $\psi = \chi$.

To propagate the wave packet $\phi(t)$, we use the Herman−Kluk-type frozen Gaussian expansion approximation,[37]

$$\phi(\mathbf{r},t) = \int_{\mathrm{traj}}\frac{3d\mathbf{q}_0\,\mathrm{d}\mathbf{p}_0}{(2\pi)^N}g(\mathbf{r};\gamma,\mathbf{q}_t,\mathbf{p}_t)\,C_{\gamma,\mathbf{q}_0,\mathbf{p}_0,t}\exp[\mathrm{i}S_{\mathbf{q}_0,\mathbf{p}_0,t}]\times \int \mathrm{d}\mathbf{r}_0\,g^*(\mathbf{r}_0;\gamma,\mathbf{q}_0,\mathbf{p}_0)\,\Phi_I(\mathbf{r}_0) \tag{9}$$

where N is the dimensionality of configuration space, $S_{\mathbf{q}_0,\mathbf{p}_0,t}$ is the classical action along the trajectory from ($\mathbf{q}_0$, $\mathbf{p}_0$, $t = 0$) to ($\mathbf{q}_t$, $\mathbf{p}_t$, t), and $C_{\gamma,\mathbf{q}_0,\mathbf{p}_0,t}$ is the Herman−Kluk pre-exponential factor along the trajectory.[37] Here the frozen Gaussian wave packets $g(\mathbf{r};\gamma,\mathbf{q},\mathbf{p})$ are defined as

$$g(\mathbf{r};\boldsymbol{\gamma},\mathbf{q},\mathbf{p}) = \prod_{j=1}^{N}\left(\frac{2\gamma_j}{\pi}\right)^{N/4}\exp\left[-\gamma_j(r_j - q_j)^2 + \frac{\mathrm{i}}{\hbar}p_j(r_j - q_j)\right] \tag{10}$$

where γ_j is a constant parameter common for all wave packets. The above expression for $\phi(\mathbf{r},t)$ is explained as follows: The initial wave function Φ_I is expanded in terms of the frozen Gaussian wave packets, and each packet is propagated by classical mechanics with its shape kept fixed. The final wave function is expressed as a sum of thus propagated frozen Gaussians multiplied by the factors $C_{\gamma,\mathbf{q}_0,\mathbf{p}_0,t}\exp[\mathrm{i}S_{\mathbf{q}_0,\mathbf{p}_0,t}]$. The initial conditions of classical trajectory ($\mathbf{q}_0$, $\mathbf{p}_0$) are selected by the Monte Carlo procedure. The wave packet $\chi(t)$ is expanded in a similar way at $t = T$ and is propagated backward from Φ_T. The action integral S and the pre-exponential factor C are defined as

$$S_{\mathbf{q}_0,\mathbf{p}_0,t} = \int_0^t\left[\sum_{j=1}^{N}\frac{p_{j,\tau}}{2m_j} - V(\mathbf{q}_\tau)\right]\mathrm{d}\tau \tag{11}$$

and

$$C_{\gamma,\mathbf{q}_0,\mathbf{p}_0,t} = \pm\sqrt{\frac{1}{2}\left[\frac{\partial\mathbf{q}_t}{\partial\mathbf{q}_0} + \gamma^{-1}\frac{\partial\mathbf{p}_t}{\partial\mathbf{p}_0}\gamma + \frac{\mathrm{i}}{2\hbar}\gamma^{-1}\frac{\partial\mathbf{p}_t}{\partial\mathbf{q}_0} - 2\mathrm{i}\hbar\frac{\partial\mathbf{q}_t}{\partial\mathbf{p}_0}\gamma\right]} \tag{12}$$

where γ is the diagonal matrix composed of the parameters γ_j.

The correlation function $\Theta_k(t)$ is now expressed as

$$\Theta_k(t) = \int_{\mathrm{traj}}\frac{\mathrm{d}\mathbf{q}_0\,\mathrm{d}\mathbf{p}_0}{(2\pi\hbar)^N}C^*_{\gamma,\mathbf{q}_0,\mathbf{p}_0,t}\exp\left[-\frac{\mathrm{i}}{\hbar}S_{\mathbf{q}_0,\mathbf{p}_0,t}\right]\times \langle\phi(0)|g_{\gamma,\mathbf{q}_0,\mathbf{p}_0}\rangle\Omega_k(\gamma,\mathbf{q}_t,\mathbf{p}_t) \tag{13}$$

where

$$\Omega_k(\gamma,\mathbf{q}_t,\mathbf{p}_t) = \int_{\mathrm{traj}}\frac{\mathrm{d}\mathbf{q}'_0\,\mathrm{d}\mathbf{p}'_0}{(2\pi\hbar)^N}\left\langle g_{\gamma,\mathbf{q}_t,\mathbf{p}_t}\middle|\mu_k(\mathbf{r})\middle|g_{\gamma,\mathbf{q}'_0,\mathbf{p}'_0}\right\rangle C_{\gamma,\mathbf{q}'_0,\mathbf{p}'_0}\times \exp\left[\frac{\mathrm{i}}{\hbar}S_{\mathbf{q}'_0,\mathbf{p}'_0,t}\right]\left\langle g_{\gamma,\mathbf{q}'_0,\mathbf{p}'_0}\middle|\chi(0)\right\rangle \tag{14}$$

Since the wave functions $\phi(t)$ and $\chi(t)$ are expanded in terms of classical trajectories, the correlation function $\Theta_k(t)$ contains the double summation with respect to these trajectories. This is still very much computationally demanding. We avoid this by taking only those trajectories that run close to each other. This is equivalent to the linearization of classical dynamics:

$$\mathbf{q}'_t \simeq \mathbf{q}_t + \frac{\partial\mathbf{q}_t}{\partial\mathbf{q}_0}\delta\mathbf{q}_0 + \frac{\partial\mathbf{p}_t}{\partial\mathbf{p}_0}\delta\mathbf{p}_0 \tag{15}$$

and

$$\mathbf{p}_t' \simeq \mathbf{p}_t + \frac{\partial \mathbf{p}_t}{\partial \mathbf{q}_0}\delta\mathbf{q}_0 + \frac{\partial \mathbf{p}_t}{\partial \mathbf{p}_0}\delta\mathbf{p}_0 \tag{16}$$

with $\delta\mathbf{q}_0 = \mathbf{q}_0' - \mathbf{q}_0$ and $\delta\mathbf{p}_0 = \mathbf{p}_0' - \mathbf{p}_0$. The classical action S and the pre-exponential factor C are expanded to the second and the zeroth order, respectively. These approximations are the same as those used in the cellurization procedure or the linearization approximation in the semiclassical mechanics.[55−57] In the practical calculations it is usually possible to expand the function $\chi(0)$ in terms of the same Gaussian functions and the factor $\langle g_{\gamma,\mathbf{q}_0'\mathbf{p}_0'}|\chi(0)\rangle$ can be simply analytically evaluated. Furthermore, if the dipole moment $\mu_k(\mathbf{r})$ can be assumed to be a linear function of $\mathbf{r}$ within the spread of the wave packet, the correlation function can be finally very much simplified as

$$\Theta_k(t) = \int_{\text{traj}} \frac{d\mathbf{q}_0\, d\mathbf{p}_0}{(2\pi\hbar)^N}\langle\phi(0)|g_{\gamma,\mathbf{q}_0,\mathbf{p}_0}\rangle\langle g_{\gamma,\mathbf{q}_0,\mathbf{p}_0}|\chi(0)\rangle[\mu_k(\mathbf{q}_t) - \nabla\mu_k(\mathbf{q}_t)\mathbf{F}_{\gamma,\mathbf{q}_0,\mathbf{p}_0,t}] \tag{17}$$

where $\mathbf{F}_{\gamma,\mathbf{q}_0,\mathbf{p}_0,t}$ is a function of the trajectory parameters and its detailed expression is given in refs 23 and 24. If the dipole moment does not significantly vary within the width of frozen wave packet, then the second term in the square bracket is negligible and the correlation function becomes very simple. This simplifies the calculations of optimal control field very much and the method is applicable to multidimensional systems.

As mentioned in the previous section, the optimal control method is very time-consuming and ineffective, when the overlap between the initial and target states is small. Some methods to cure this defect have been proposed such as the local control scheme and the use of an intermediate target state.[20,38,39] The present semiclassical theory cannot be free from this difficulty. To overcome this difficulty, we divide the whole process into a sequence of steps and each step is optimized. In other words, the optimization procedure is performed by setting an appropriate target state in each step. This intermediate target state plays a role to guide the trial state and is not necessarily accurate, since the important factor is the final efficiency.The wave packet obtained as the result of the previous step is used as an initial state for the next step. The whole procedure can be very much accelerated by this method and now enables us to treat higher dimensional systems. We named this method the *guided optimal control theory*. In the case of the directed momentum method, the target state is spatially very close to the initial state and it is not necessary to guide.

2. Quadratic Frequency Chirping. In the simplest case of two energy levels, the transition probability after n periods of oscillation of laser frequency astride the crossing point is given by (see Chapter 13 of ref 5 and also refs 25 and 10)

$$P_{12}^{(n)} = 4\frac{\sin^2(n\xi)}{\sin^2(\xi)}p(1-p)\sin^2\psi \tag{18}$$

where

$$\cos\xi = (1-p)\cos(2\psi - \sigma) + p\cos(\sigma) \tag{19}$$

p is the nonadiabatic transition probability for one passage of the crossing point, and ψ and σ are the phases determined from the phase along the potentials and the phase induced by the nonadiabatic transition. The condition of the complete excitation, $P_{12}^{(n)} = 1$, reduces to $\sin^2(n\xi) = 1$ and $4p(1-p)\sin^2\psi = \sin^2\xi$. The first requirement determines ξ for a given n and the second requirement gives the condition for p and ψ for a given ξ. In the one period case (quadratic chirping), the condition becomes simply $p = {}^1/_2$ and $\sin^2\psi = 1$. The three-level (one initial and two closely lying excited levels) and four-level (one initial and three closely lying excited levels) problems can be formulated analytically and the conditions for the selective and complete excitation of any one of the excited states can be derived and numerical demonstrations with use of the model systems are given in refs.[10,42]

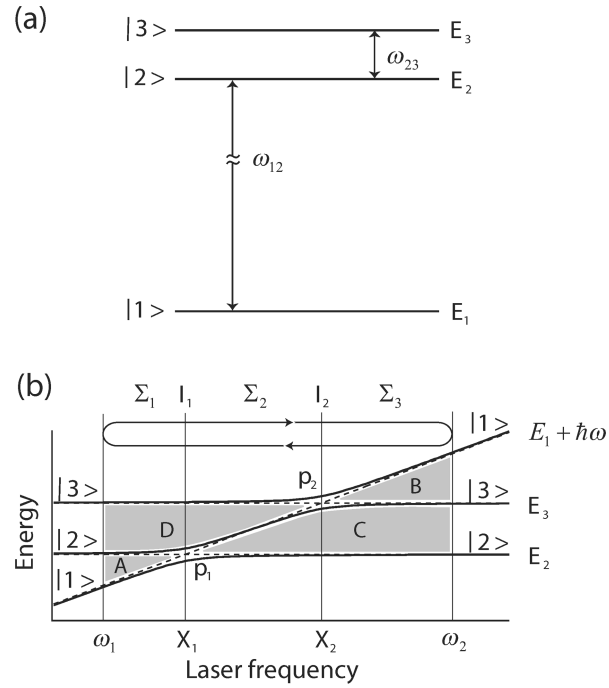

Figure 3. (a) Three-level model. (b) Floquet diagram of the three-level model shown in (a) as a function of laser frequency.

For the later convenience the basic equations are given below for the three-level case (see Figure 3). It is assumed that $\omega_{12} \gg \omega_{23}$ and the dipole transition between the excited levels is neglected, since the applied laser frequency ω is close to ω_{12}. If the laser frequency ω is swept from ω_1 to ω_2 (half period), then the transition matrix is given by

$$T_{\omega_1\to\omega_2} = \Sigma_3 I_2 \Sigma_2 I_1 \Sigma_1 \tag{20}$$

where Σ_j represents the adiabatic propagation from X_{j-1} to X_j, and I_j represents the nonadiabatic transition at the crossing X_j (see Figure 3b). They are given as

$$(\Sigma_j)_{pq} = \exp[-i\sigma_j^{(p)}]\delta_{pq} \tag{21}$$

$$\sigma_j^{(k)} = \frac{1}{\hbar}\int_{X_{j-1}}^{X_j} E_k^{(ad)}(\omega)\, dt \tag{22}$$

$$\mathbf{I}_1 = \begin{pmatrix} \sqrt{1-p_1}\exp[i\phi_1] & \sqrt{p_1}\exp[i\psi_1] & 0 \\ -\sqrt{p_1}\exp[-i\psi_1] & \sqrt{1-p_1}\exp[i\phi_1] & 0 \\ 0 & 0 & 1 \end{pmatrix} \tag{23}$$

The matrix $\mathbf{I}_2$ is similar to $\mathbf{I}_1$, representing the transition at X_2 between the adiabatic states E_2 and E_3. Here, p_j denotes the

nonadiabatic transition probability at X_j, the phases ϕ and ψ are the dynamical phases induced by nonadiabatic transition at X_j, the energy E_k is the kth adiabatic state, $X_0 = \omega_1$ and $X_3 = \omega_2$. In the case of one period of frequency oscillation (quadratic chirping) the overall transition probability from $|1\rangle$ to $|2\rangle$ is explicitly given by

$$P_{12} = p_1(1 - p_1)|\exp[2iC] - 1 + p_2(1 - \exp[-2iB])|^2 \tag{24}$$

with

$$B = \phi_2 + \psi_2 + \Delta\sigma_3^{(3,2)} \tag{25}$$

and

$$C = \phi_1 + \psi_1 - \phi_2 + \Delta\sigma_2^{(2,1)} + \Delta\sigma_3^{(2,1)} \tag{26}$$

where

$$\Delta\sigma_j^{(k,l)} = \sigma_j^{(k)} - \sigma_j^{(l)} \tag{27}$$

The condition for the selective and complete excitation to $|2\rangle$ is given by

$$p_1 = 1/2 \qquad B = m\pi \qquad \text{and} \qquad C = (n + 1/2)\pi \qquad (n, m = \text{integer}) \tag{28}$$

Similarly, the condition of the selective and complete excitation to $|3\rangle$ is obtained as

$$p_2 = 1/2 \qquad A = m\pi \qquad \text{and} \qquad D = (n + 1/2)\pi \tag{29}$$

with

$$A = \phi_1 - \psi_1 + \Delta\sigma_1^{(2,1)} \tag{30}$$

and

$$D = -\phi_1 + \phi_2 - \psi_2 + \Delta\sigma_1^{(3,2)} + \Delta\sigma_2^{(3,2)} \tag{31}$$

Phases A−D roughly correspond to the areas shown in Figure 3b.

In the case of pump/dump of the wave packet we have to take into account the spatial spread of the wave packet, and the excitation probability $\mathscr{P}$ from the initial state $V_i(\mathbf{x})$ to the excited state $V_e(\mathbf{x})$ is given by

$$\mathscr{P} = \int P_{12}(\mathbf{x})|\Psi_g(\mathbf{x}, t = 0)|^2 \, d\mathbf{x} \tag{32}$$

where $\Psi_g(\mathbf{x}, t = 0)$ is the initial wave packet and the nonadiabatic transition probability $P_{12}(\mathbf{x})$ is calculated from the corresponding two-level problem at $\mathbf{x}$. Then as usual, the probability $P_{12}(\mathbf{x})$ is expressed as

$$P_{12}(\mathbf{x}) = 4p(\mathbf{x})[1 - p(\mathbf{x})] \sin^2 \Psi(\mathbf{x}) \tag{33}$$

with

$$p(\mathbf{x}) = \exp\left[-\frac{\pi}{4\sqrt{\alpha\beta}}\left(\frac{2}{1 + \sqrt{1 + \beta^{-2}(0.4\alpha + 0.7)}}\right)^{1/2}\right] \tag{34}$$

The two basic parameters α and β to determine p and Ψ of the Zhu−Nakamura formulas are explicitly given by[10,44]

$$\alpha(x) = \frac{\hbar\alpha_\omega}{(\mu(\mathbf{x})\epsilon)^3} \tag{35}$$

and

$$\beta(\mathbf{x}) = \frac{1}{\mu(\mathbf{x})\epsilon}\left[\Delta(\mathbf{x}) - \hbar\beta_\omega + \frac{(\vec{v} \cdot \nabla\Delta(\mathbf{x}))^2}{4\hbar\alpha_\omega}\right] \tag{36}$$

where $\mu(\mathbf{x})$, ϵ, and $\vec{v}$ are the transition dipole moment, laser intensity, and mean velocity of the wave packet, respectively,

$$\Delta(\mathbf{x}) = V_e(\mathbf{x}) - V_i(\mathbf{x}) \tag{37}$$

and α_ω and β_ω are the chirping rate and the carrier frequency; i.e., the laser frequency $\omega(t)$ is given by

$$\omega(t) = \alpha_\omega(t - t_p)^2 + \beta_\omega \tag{38}$$

The laser parameters have to be chosen so that α and β make the transition probability as close to unity as possible. It is recommended to make α and β sitting in the following ranges to achieve nearly complete excitation.

$$0.7 \lesssim \alpha \lesssim 2.0 \qquad \text{and} \qquad 0.5 \lesssim \beta \lesssim 1.2 \tag{39}$$

The selective and complete excitation of atomic fine structures by using the quadratic chirping is numerically demonstrated in section IV.3, by taking the real atoms K and Cs. In the latter case a two-photon process is required, but there is no difficulty. In section IV.4, control of the photodissociation of OHCl molecule is demonstrated by using the quadratic chirping and the directed momentum methods. This presents an example of excitation of the wave packet by the quadratic chirping.

IV. Numerical Demonstrations

1. Full Dimensional Vibrational Isomerization of HCN. The isomerization or dissociation dynamics of HCN has been considered either with only small number of degrees of freedom taken into account[58,59] or by using purely classical methods (see ref 60 and references therein). The process of NCH−HNC isomerization occurs without change of electronic state, and thus what we have to control is the nuclear motion on a single adiabatic potential energy surface together with the molecular rotation. For the calculations to be realistic, the intensity of the controlling field should not be so high as to cause tunneling ionization, multiphoton electronic excitation, or dissociation. The maximal value of the intensity of the laser pulse that could be

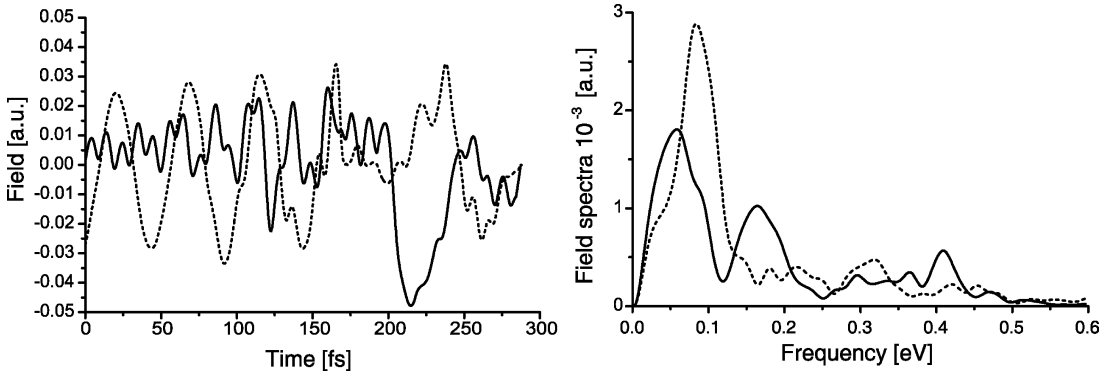

Figure 4. Optimal field with the zero frequency component removed (left) and its spectra (right). Solid line: component along the *X*-axis. Dashed line: component along the *Y*-axis.

used to manipulate the HCN molecule without any damage through ionization in the IR region is estimated to be $\sim 10^{14}$ W/cm^2,[58] which corresponds to the field amplitude of 0.05 (atomic units). This requirement results in longer controlling duration, and the rotation of molecule as a whole should be controlled at the same time. Thus the present treatment is a full six-dimensional calculation.

The HCN molecule is described in terms of two three-dimensional vectors:[61] $\mathbf{R}_{N=C}$ for the vector from N to C and $\mathbf{R}_H$ for the vector from the center of mass of CN to H. The space-fixed Cartesian framework is used with the *X*-axis set to be parallel to the initial direction of $\mathbf{R}_{N=C}$ and the *Y*- and *Z*-axes perpendicular to it. The centers of mass of NC and of the whole system are assumed to be the same so that the kinetic energy part of the Hamiltonian is diagonal. The molecule is assumed to be aligned after some laser-induced process.[58] The potential energy surface and dipole moment are taken from ref 62. The ground state wave packets for the HCN and CNH configurations are approximated by Gaussian functions centered (in atomic units) at $\mathbf{R}_{N=C} = (2.1785, 0.0, 0.0)$, $\mathbf{R}_H = (3.1855, 0.0, 0.0)$ and $\mathbf{R}_{N=C} = (2.197, 0.0, 0.0)$, $\mathbf{R}_H = (-2.875, 0.0, 0.0)$, respectively. The width parameters are calculated to fit to the principal modes of the potential wells.

According to the idea of guided control, the whole process is divided into the following two main procedures:[61] (i) acceleration of the initial wave packet in the HCN configuration so that it can pass the interstate barrier and (ii) deceleration of the wave packet so that it stays in the target region. The field intensity is monitored at each step and if its maximum amplitude exceeds the value of 0.05 (atomic units), it is reduced to that value by multiplying an appropriate factor. The spectrum of the controlling field typically contains one main peak and several harmonics with lower intensity. These secondary peaks are adjusted by this intensity reduction procedure. When the intensity is thus reduced, the controlling time duration should also be changed to maximize the control efficiency. By repeating computations for different time durations *T*, we can find the best one. The shortest duration for the maximum efficiency under the intensity lower than the inonization threshold is finally found to be 288 fs, where the acceleration lasts for 168 fs and the deceleration lasts for 120 fs.

The acceleration procedure in turn is further divided into the following three steps with intermediate target states of Gaussian wave packets with the same central coordinates and width parameters as those of the initial wave packet, but with the following different central momenta for each step (in atomic units): $\mathbf{P}_{N=C} = (0.0, -15.0, 0.0)$ and $\mathbf{P}_H = (0.0, 10.0, 0.0)$ for the first step, $\mathbf{P}_{N=C} = (0.0, -22.5, 0.0)$ and $\mathbf{P}_H = (0.0, 15.0, 0.0)$ for the second, and $\mathbf{P}_{N=C} = (0.0, -29.2, 0.0)$ and $\mathbf{P}_H = (0.0, 20.0, 0.0)$ for the third. The optimization procedure for the first step is carried out with zero initial guess field. The field obtained as a result of the previous step is used as an initial guess field for the next.

Similarly, to decelerate the wave packet so that it stays in the CNH target configuration potential well, the three-step optimization procedure is used, but in a bit different way. The initial guess field is zero for each step, and the wave packet obtained as a result of the previous step is set to be an initial state for the next. The actual wave packet that can energetically pass over the CNH potential well should be decelerated by the first step so that it hits the opposite side of the potential well and starts to move backward. We set the first intermediate target state to be the same as the ground state wave packet in the potential well corresponding to CNH with counterclockwise rotation for a certain angle. This angle and time duration of the first step is adjusted so that the wave packet is decelerated enough to stay in CNH potential and the controlling field intensity is lower than the ionization threshold. The suitable values found are 26° for the angle and 40 fs for the correspondent duration. The intermediate target states for the second and third steps are set to be the ground state wave packet in the potential well corresponding to CNH turned clockwise for 26°. These states are set to follow clockwise rotation of the heavy NC bond, which occurs during the isomerization. The each step takes 40 fs.

The number of trajectories used at each step of control is kept to be 100 000. Typically, the convergence is achieved by about five iterations at each step. The final isomerization probability is calculated by the formula

$$P_{iso} = \langle \phi(T) | h(0.35 - \cos\theta) | \phi(T) \rangle \qquad (40)$$

where θ is the angle between $\mathbf{R}_{N=C}$ and $\mathbf{R}_H$, $h(x) = 1$ for $x \geq 0$ and 0 for $x < 0$, and $\cos\theta = 0.35$ corresponds to the saddle point between the HCN and CNH configurations. The final isomerization efficiency attained is 74%. It should be noted, however, that the time average of the field turns out to be nonzero, which means that the zero-frequency component exists. The field with this zero-frequency component removed out and its spectrum are shown in Figure 4. Since the system remains symmetric along the *XY* plane, it has no dipole moment in the direction of *Z*-axis. As a result, the *Z*-component of the field is zero. The snapshots of the wave packet driven by the controlling field at various times are shown in Figure 5. The removal of the zero-frequency component reduces the isomerization ef-

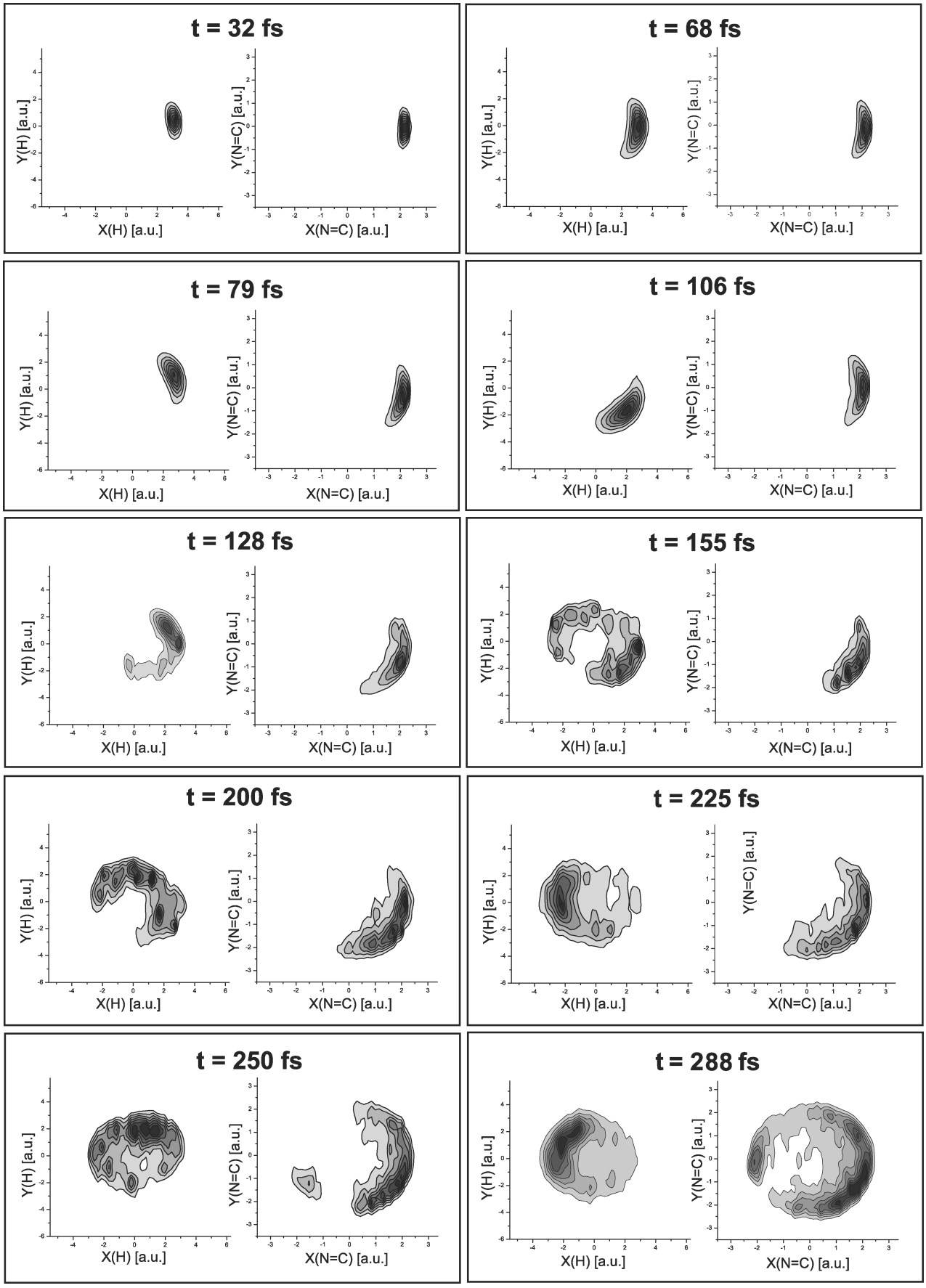

Figure 5. Snapshots of the wave packet in the HCN−CNH isomerization driven by the controlling field at various times. The probability density is given at each figure as a function of proton coordinate (left) and N═C bond vector coordinate (right).

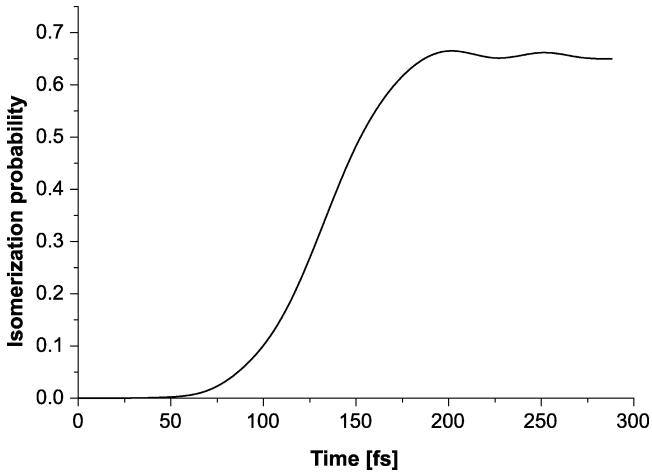

Figure 6. HCN−CNH isomerization probability calculated as a function of time.

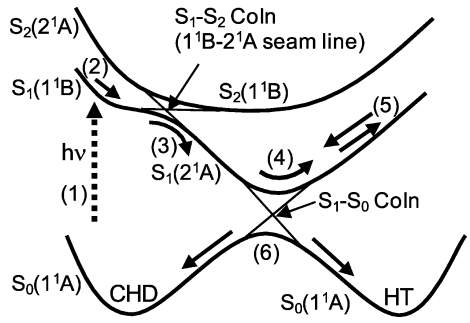

Figure 7. Reaction scheme of CHD/HT photoisomerization taken from ref 66. (1) CHD is photoexcited to $S_1(1^1B)$ (0 fs), (2) ring-opening (C−C bond breaking) proceeds descending the $S_1(1^1B)$ PES, (3) electronic state character of S_1 changes from 1^1B to 2^1A at the 1^1B-2^1A seam line (∼20 fs), (4) $S_1(2^1A)$ wave packet ascends the PES toward the open-ring direction due to the excess kinetic energy from the Franck−Condon (FC) region, where the wave packet is still compact and does not spread over the S_1-S_0 conical intersection, (5) wave packet turns back toward the closed-ring direction (∼70 fs), and (6) wave packet is scattered by the steep potential slope at the closed-ring (100−130 fs), then radiationless decay to S_0 occurs (130−180 fs) through the S_1-S_0 conical intersection located along the direction toward the 5-membered ring (5MR).

ficiency by 9%. The time variation of the isomerization probability is shown in Figure 6.

2. Cyclohexadiene (CHD)/Hexatriene(HT) Photoisomerization. As is well-known, molecules can manifest various functions such as photochromism, molecular switches, and memories.[63−65] Actually, this represents one of the important subjects in nanoscience. In the present subsection, the reaction control scheme of the photoswitching molecules with the intense laser is theoretically investigated using the idea of preparation of an initial wave packet on the ground state with appropriately directed momentum. The main purpose here is to demonstrate the possibility of enhancing the transition at the conical intersection by taking the CHD/HT photoconversion as an example.

Figures 7 and 8 schematically show the reaction dynamics of the CHD/HT photoisomerization clarified in ref 66 by using the wave packet dynamics on the ab initio PESs starting from the Franck−Condon region at CHD, where the two-dimensional reduced coordinates (Figure 9A) are employed. These represent the ring-opening reactive coordinates. The reader should refer to ref 66 for the details of the quantum chemical and dynamics computations. In the vicinity of the conical intersection, the full-dimensional semiclassical analysis of nonadiabatic transitions are also made on the basis of the harmonic normal mode approximation to correct the overestimation of the nonadiabatic transition probabilities due to the reduced dimensionality.[66] We use the notations in C_2 symmetry to indicate the electronic state characters such as 1^1A, 2^1A, and 1^1B for convenience. Note that the actual computation was performed in the C_1 symmetry, because the true conical intersection was found in the C_1 symmetry. The PESs, diabatic couplings and transition dipole moments of the CHD/HT system have been determined by ab initio calculations using the multireference configuration interaction (MRCI) method. The kinetic energy operator along the Jacobi coordinates (Figure 9A) is expressed as follows

$$\hat{T} = -\frac{1}{2\mu_R}\frac{\partial^2}{\partial R^2} + \frac{\hat{j}^2}{2\mu_R R^2 + 2\mu_r r^2} \qquad (41)$$

where $\mu_R(\mu_r)$ and $\hat{j}$ are the reduced mass of $R(r)$ and angular momentum for θ, respectively. The distance r is the C_5-C_6 bond length and is fixed at 1.4 Å. The θ is the angle between R and r. The other coordinates are optimized using the complete active space SCF(CASSCF) energy gradient. The diabatization procedure is used in the wave packet dynamics. The dynamics of the natural CHD/HT photoisomerization is summarized as follows (see Figures 7 and 8):

(1) The equilibrium wave packet (vibrational ground state) on the electronic ground (S_0) state in the CHD region is photoexcited to the $S_1(1^1B)$ electronic state and then descends the PES toward the open-ring direction (steps 1 and 2 in Figure 7).

(2) The $S_1(1^1B)$ wave packet encounters the S_1-S_2 conical intersection located along the C_2 symmetric pathway (Figure 8A), at which the major portion (∼80%) changes the character from 1^1B to 2^1A staying on the S_1 adiabatic state.

(3) The $S_1(2^1A)$ wave packet goes to the open-ring region due to the excess kinetic energy from the Franck−Condon region and turns back toward the closed-ring region due to the gently ascending potential slope (Figure 8B), where the wave packet is still compact and does not spread over the S_1-S_0 CoIn (the structure of the S_1-S_0 conical intersection is shown in Figure 9B).

(4) The wave-pakcet is scattered by the steep potential slope at the closed-ring region and reaches the S_1-S_0 conical intersection located along the direction toward the 5MR (Figure 8B).

(5) Finally, the first nonadiabatic transition to S_0 occurs through the S_1-S_0 conical intersection and the S_0 wave packet bifurcates into the CHD and HT regions (step 6 in Figure 7).

This reaction dynamics reasonably explains the experimentally observed ultrafast $S_1 \rightarrow S_0$ decay (130 fs).[67] The CHD:HT branching ratio after the $S_1 \rightarrow S_0$ decay is approximately ∼5:5 in the wave packet dynamics.[66] This is because the S_1-S_0 conical intersection (Figure 9B) is located at the halfway ridge between the CHD and HT basins on the S_0 PES (Figure 8B), where the wave packet is rather delocalized when crossing the S_1-S_0 conical intersection compared to the initial one in the FC region. The experimental CHD:HT branching ratio is ∼6:4 in solution.[68] The results of the previous wave packet dynamics[66] are generally consistent with the experiments.[67,68]

On the basis of the wave packet dynamics mentioned above, we can propose the following control scheme to increase the photoisomerization efficiency by (i) preparing the initial wave packet with the directed momentum toward the 5MR in the CHD

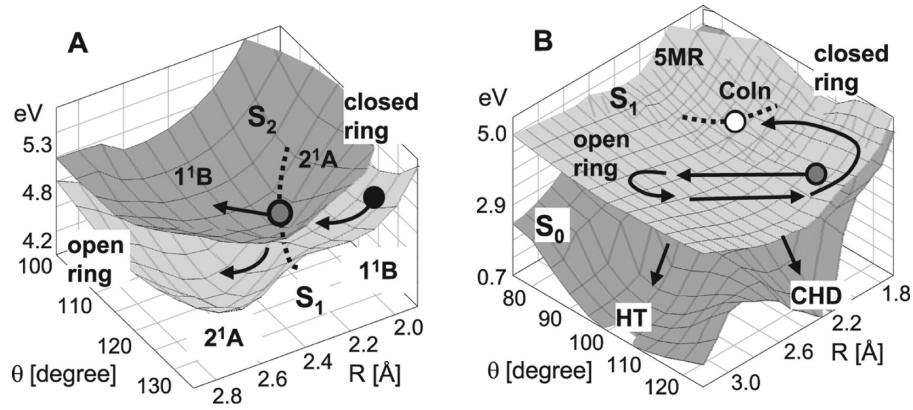

Figure 8. (A) S_1-S_2 and (B) S_1-S_0 coupled PESs along the two-dimensional Jacobi coordinates. The black, gray, and white circles and dotted lines indicate the locations of the FC region, S_1-S_2 conical intersection minimum, 5MR S_1-S_0 conical intersection minimum, and seam lines, respectively, taken from ref 66. The solid arrows indicate the schematic wave packet pathway of natural photoisomerization starting from the vibrational ground state.

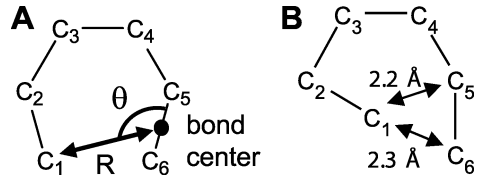

Figure 9. (A) Two-dimensional Jacobi coordinates used in the wave packet dynamics. (B) Schematic molecular geometry at the 5MR S_1-S_0 conical intersection minimum (the minimum on the conical intersection hypersurface).

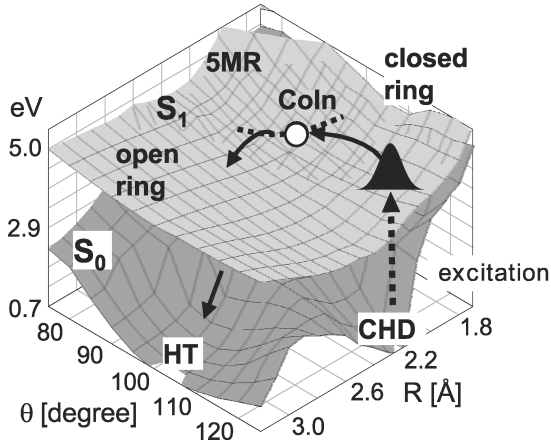

Figure 10. S_1-S_0 coupled PESs along the two-dimensional Jacobi coordinates. The white circle and dotted line indicate the locations of 5MR S_1-S_0 CoIn minimum and seam line, respectively. The solid arrows indicate the schematic wave packet pathway accelerated toward the 5MR.

potential basin on the S_0 electronic state and (ii) achieving nearly complete electronic excitation to $S_1(1^1B)$ (step 1 in Figure 7) with use of the quadratically chirped pulse (see Figure 10). These methods enable us to control the motion of the wave packet at the S_1-S_0 CoIns and enhance the HT/CHD branching ratio. Some other methods have also been proposed to change the wave packet momentum such as the cyclic pump/dump method.[69,70] The present method is more direct using only a single potential energy surface.

To calculate the controlling laser field to prepare the appropriately accelerated wave packet in the CHD potential basin on the S_0 electronic state, the method of optimal control is used. The initial state is the ground vibrational state of the CHD configuration potential minimum. The target state is set to be a Gaussian wave packet with the same central coordinates and width parameters as those of the initial wave packet, but with the different central momenta $\mathbf{P}_R = -16.21$ and $\mathbf{P}_\theta = -39.25$ atomic units. This correponds to the ~6 kcal/mol kinetic energy directed toward the 5MR. The acceleration duration is set to be 400 fs. The optimal control field and its spectra are shown in Figure 11. The efficiency of control achieved is ~93%.

This accelerated wave packet can be efficiently excited to the $S_1(1^1B)$ state by using the quadratically chirped pulse. Approximately 90% excitation is achieved at a laser istensity of about 3.5 TW/cm^2. The wave packet on $S_1(1^1B)$ goes toward the 5MR due to the initial momentum, even though the $S_1(1^1B)$ PES is downhill along the C_2 symmetric ring-opening direction.[66] The electronic state character changes to $S_1(2^1A)$ at the 1^1B-2^1A seam line (step 3 in Figure 7). Since the wave packet pathway toward the 5MR (Figure 10) is far from the S_1-S_2 conical intersection located on the C_2 symmetric pathway (Figure 8A),[66] the nonadiabatic transition to $S_2(1^1B)$ is negligible. The S_1 wave packet directly goes to the S_1-S_0 conical intersection due to the initial momentum toward the 5MR without any excursions around the open-ring region (i.e., skipping the steps 4 and 5 in Figure 7). Figure 12A shows the changes in the wave packet populations on S_1 and S_0. The first nonadiabatic transition to S_0 rapidly occurs in 20−30 fs from the photoexcitation, keeping the wave packet compact. The S_1 and S_0 PESs are uphill toward the 5MR and thus the wave packet turns around toward the CHD or HT product region. Most part of the S_0 wave packet goes down to HT after the $S_1 \rightarrow S_0$ decay (Figure 12A), because the group velocity of the wave packet is directed toward HT. This trend is qualitatively similar to the wave packet dynamics of the ring closure by Geppert et al.[71] (CHD is selectively produced). Although the 5MR S_1-S_0 conical intersection is located at the halfway ridge between the CHD and HT potential basins, the desired product can be selectively produced due to the directed momentum crossing the conical intersection. Figure 12B shows the 5:5 CHD:HT ratio by the wave-pack dynamics without any initial acceleration.[66] The comparison with Figure 12A clearly demonstrates the increase of HT production by the present scheme. The $S_1 \rightarrow S_0$ decay through the C_2 symmetric conical intersection, different from the above-mentioned 5MR S_1-S_0 conical intersection, might also occur, even though this C_2 symmetric S_1-S_0 conical intersection is less stable than the 5MR S_1-S_0 conical intersection.[70−72] The wave packet acceleration/deceleration along the C_2 symmetric ring-opening direction is possible on the basis of the cyclic pump-dump around the Franck−Condon

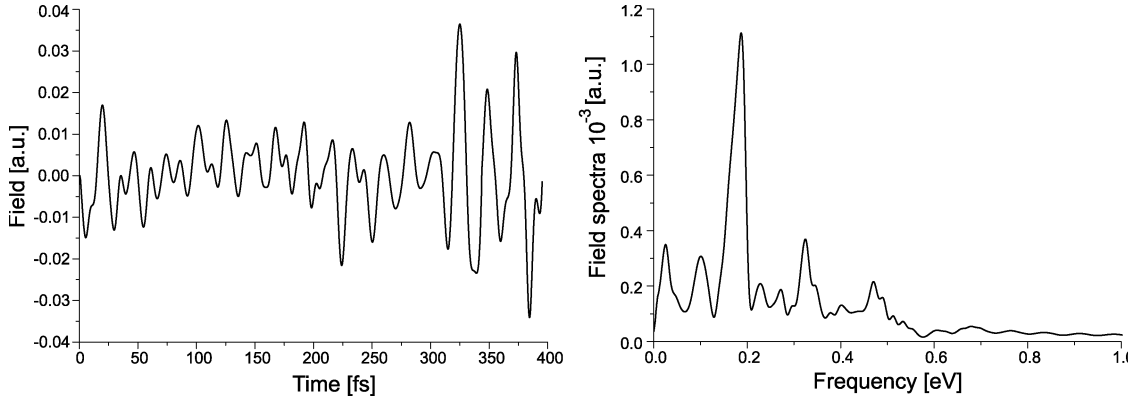

Figure 11. Optimal field for wave packet acceleration of cyclohexadiene (left) and its spectrum (right).

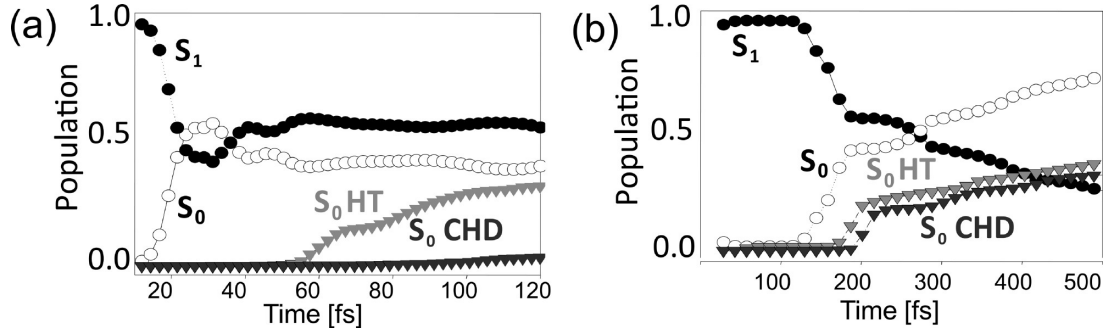

Figure 12. (A) Changes in wave packet populations on S_1 and S_0 (at HT and CHD basins) after the initial excitation of the wave packet with the directed momentum toward the 5MR and (B) those without the acceleration (i.e., excitation from the vibrational ground state) for comparison taken from ref 66.

region due to the C_2 symmetric PESs landscapes.[71] However, our wave packet dynamics considering the S_1-S_2 coupled PESs have revealed that a node along the C_2 symmetric direction appears for the S_1 wave packet after adiabatically passing the S_1-S_2 conical intersection due to the Berry phase.[66] Consequently, the C_2 symmetric S_1-S_0 conical intersection is considered to be less accessible from the Franck−Condon region at CHD compared to the 5MR one. Thus the efficient $S_1 \rightarrow S_0$ decay by the first conical intersection crossing is crucial to increase the selective production of HT, as demonstrated in the present calculations.

As was mentioned at the end of section II.2, the accelerating laser field is parallel to the derivative of the dipole moment vector in the direction of the desirable momentum. The present computations clearly demonstrate the theoretical possibility of enhancing the photoconversion efficiency by using the quadratic chirping and directed momentum methods.

3. Selective and Complete Excitation of Atomic Fine Structure Levels. The broad bandwidth of the short pulse laser is an essential property for quantum control, since it can induce various transitions. When it comes to selective excitation, however, the broad band laser should be appropriately pulse shaped to kill undesired transitions. The well-known scheme of selective excitation is the Ramsey fringe[73,74] in which a pair of pulses having specific delay time and phase difference are utilized to control the interference effect. It should be noted, however, that this scheme is based on a perturbative framework, and it is applicable only when the transition probability is sufficiently small compared to unity. Our scheme utilizing the quadratic chirping discussed in section III.2, on the other hand, is applicable to nonperturbative regime, and selective transition to any one of the closely lying states is possible with unit probability. In our scheme of quadratic chirping in the case of two closely lying excited levels (three-level system), there are four temporally separated transitions at four crossing points. Selectivity can be realized by designing the destructive interference at the exit to the undesired state, namely, at the third crossing.

As examples to demonstrate the effectiveness of our scheme of the quadratic chirping discussed in section III.2, here we take the selective excitation to one of the closely lying fine structure states of K and Cs atoms. We have calculated the time variation of population of each state by solving the time-dependent coupled Schrödinger equations with the total wave function expanded in terms of the unperturbed atomic eigen states. In the case of the K(Cs) atom, 10(18) eigenstates are used in the expansion and the convergence of the numerical results is confirmed. Figure 13a shows the time variation of populations of the ground 4S (solid line), and excited $4P_{1/2}$ (dashed line) and $4P_{3/2}$ (dotted line) states of K. The laser intensity is 0.36 GW/cm^2 with a quadratic frequency chirping shown in Figure 13b. The chirping is concave down, which makes it possible to completely suppress the transition to the upper excited state and realize the selective excitation to the lower excited state ($4P_{1/2}$) with 100% efficiency. The excitation energies of the K atom from the ground state to $4P_{1/2}$ and $4P_{3/2}$ are 12 985.17 and 13 042.88 cm^{-1}, respectively, and thus the energy splitting between them is equal to $\Delta E = 57.7$ cm^{-1}. This energy splitting corresponds to the time, $\Delta T = 2\pi/\Delta E \sim 577$ fs by the uncertainty principle. As seen from Figure 13a, the quadratic chirping scheme enables us to achieve the complete and selective excitation within 600 fs that is very close to ΔT. It should be noted that the ultrafast selective excitation can be achieved even faster than the uncertainty principle limit, as experimentally demonstrated in ref 74 and as utilized to propose a new spectroscopic method with quantum control.[75] This kind of ultrafast selection, however, can attain a transition probability much smaller than unity. It should be emphasized again that

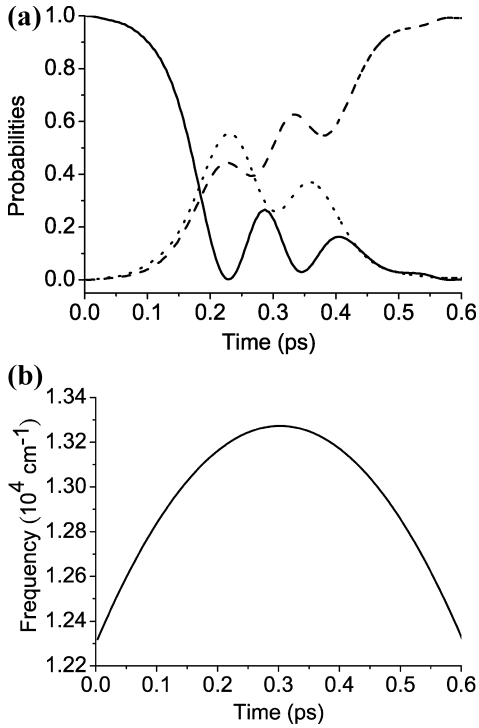

Figure 13. (a) Time variation of the populations of the ground 4S (solid line) and excited $4P_{1/2}$ (dashed line) and $4P_{3/2}$ (dotted line) states of K atom. (b) Time-dependent frequency to induce the selective excitation to $4P_{1/2}$ state.

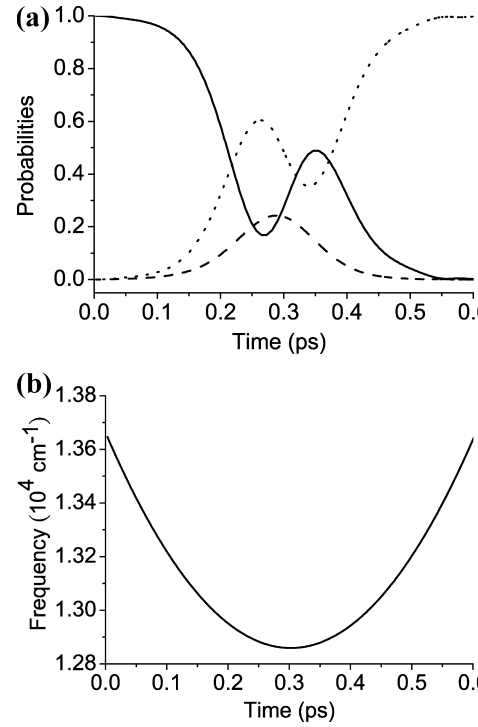

Figure 14. (a) Time variation of the populations of the ground 4S (solid line) and excited $4P_{1/2}$ (dashed line) and $4P_{3/2}$ (dotted line) states of K atom. (b) Time-dependent frequency to induce the selective excitation to $4P_{3/2}$ state.

our scheme here realizes selective excitation with *unit* probability as quickly as the uncertainty principle limit. Selective excitation to the upper ($4P_{3/2}$) state can be achieved with use of concave-up chirping instead of concave-down, as is in Figure 14. The laser intensity is 0.13 GW/cm^2, which is about 3 times smaller than the previous case. This is because the transition dipole moment between the ground and the upper excited state is larger than that between the ground and the lower excited state.

Let us consider the second example. That is the selective excitation of Cs atom from its ground state (6S) to any one of the excited states ($7D_{3/2}$ and $7D_{5/2}$). The excitation energies are 26 047.86 and 26 068.83 cm^{-1}, respectively, which are roughly 2 times larger than those of the previous K case. Thus, considering the symmetry of the excited states also, we have to employ two-photon processes. As long as the transitions (or avoided crossings) are separated in time, there is no difficulty in achieving the selection. Figure 15a shows the time variation of populations of the ground 6S (solid line) and excited $7D_{3/2}$ (dashed line) and $7D_{5/2}$ (dotted line) states of Cs. The laser intensity is 4.8 GW/cm^2, and the frequency chirping is depicted in Figure 15b. As clearly seen in Figure 15a, the complete and selective excitation to the $7D_{3/2}$ (lower) state is achieved by the concave-down quadratic chirping. Here the frequency is chirped around the half of the resonance, namely, $\sim$13 000 cm^{-1}, because the transitions take place by the two-photon absorption. The control is accomplished in 3 ps, which is roughly twice as long as the uncertainty principle limit given by $\Delta T = 2\pi/\Delta E \sim 1.6$ ps. Although our control scheme works well no matter whether it is one- or two-photon process, it is difficult to achieve complete and selective excitation in the case of the two-photon process as quickly as the uncertainty principle limit allows, as in the case of K. The reason is as follows. To induce two-photon transitions, a larger laser intensity is required, which may cause off-resonance transitions. In our case of Cs, the off-resonance

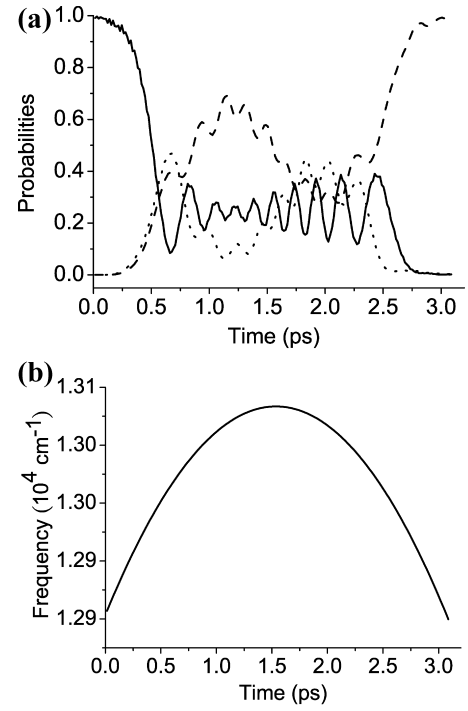

Figure 15. (a) Time variation of the populations of the ground 6S (solid line) and excited $7D_{3/2}$ (dashed line) and $7D_{5/2}$ (dotted line) states of Cs atom. (b) Time-dependent frequency to induce the selective excitation to $7D_{3/2}$ state.

excitation to 6P states becomes non-negligible when the laser intensity exceeds 5 GW/cm^2. Since the present analytical formulation given in section III.2 is for three-level problems, the laser intensity should be small to suppress these undesired transitions. To satisfy the condition $p = {}^1/_2$ with a small laser intensity, a long transition time is necessary. This is why the

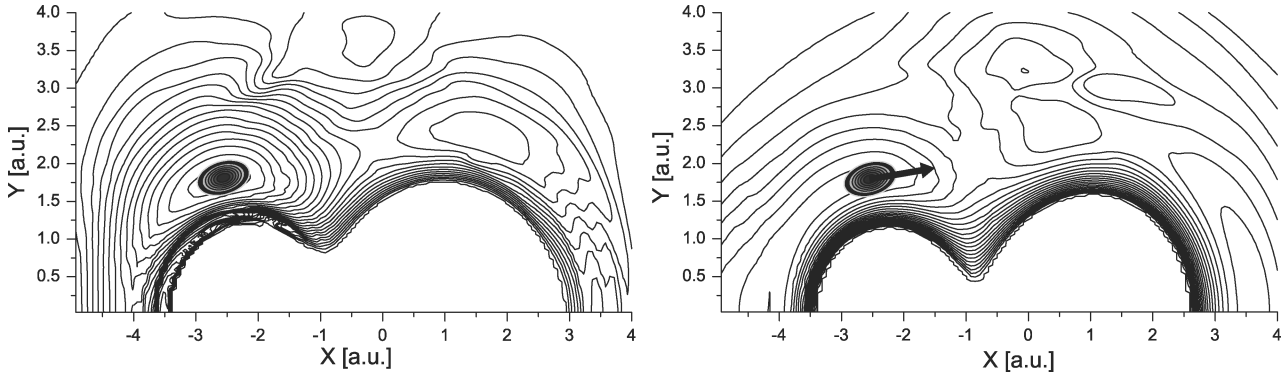

Figure 16. Potential energy surfaces of 1A′ (left) to 2A′ (right) states of OHCl as functions of proton coordinated together with ground state wave packet. Left: 1A′ potential energy surface and ground state wave packet. The arrow in the right figure shows the direction of accelleration. The *X*-axis is parallel to the initial direction of the O−Cl bond.

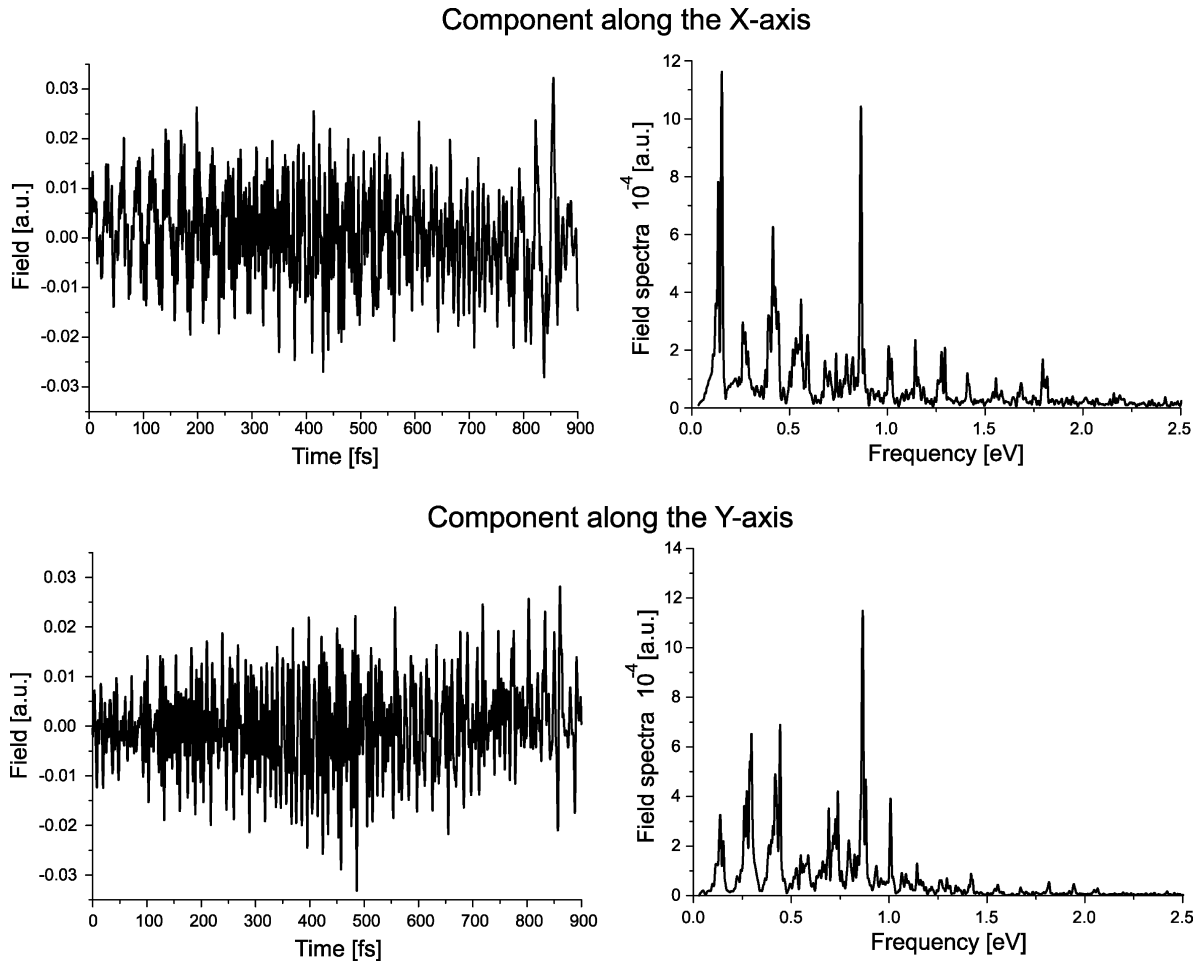

Figure 17. Optimal field found for OHCl wave packet acceleration (left) and its spectrum (right).

long control time is required. Faster selective excitation may be possible by utilizing higher order chirping,[42,43] because it can suppress the transitions to undesired states. It should also be noted that although the analytical formulation is limited to four-level systems, the idea of complete and selective excitation by the periodic chirping is general and applicable to multilevel systems, for instance, by using a numerical simulation method.

4. Control of Photodissociation of OHCl. The bond selective photodissociation of OHCl to O + HCl can be achieved with high efficiency by the following procedures: (i) appropriately accelerate the ground state wave packet using the method of the guided optimal control theory and (ii) excite the thus prepared wave packet from the ground (1A′) to the excited (2A′) state using a quadratically chirped laser pulse.

We invoke the nonrotating approximation based on the fact that the time scale of control of about 1.0 ps is much less than the rotation period of the molecule, which is about 32 ps. This provides us the following 4D model in which the rotation of the whole molecule is allowed in the molecular plane. The molecule is described in terms of two two-dimensional vectors: $\mathbf{R}_{O=Cl}$ for the vector from O to Cl and $\mathbf{R}_H$ for the vector from the center of mass of OCl to H. The space fixed Cartesian framework is used with the *X*-axis set to be parallel to the initial direction of $\mathbf{R}_{O=Cl}$ and the *Y*-axis perpendicular to it. The centers of mass of OCl and of the whole system are assumed to be the same so that the kinetic energy part of the Hamiltonian is diagonal. The potential energy surface and dipole moment are taken from ref 76. The ground state wave packet is approximated

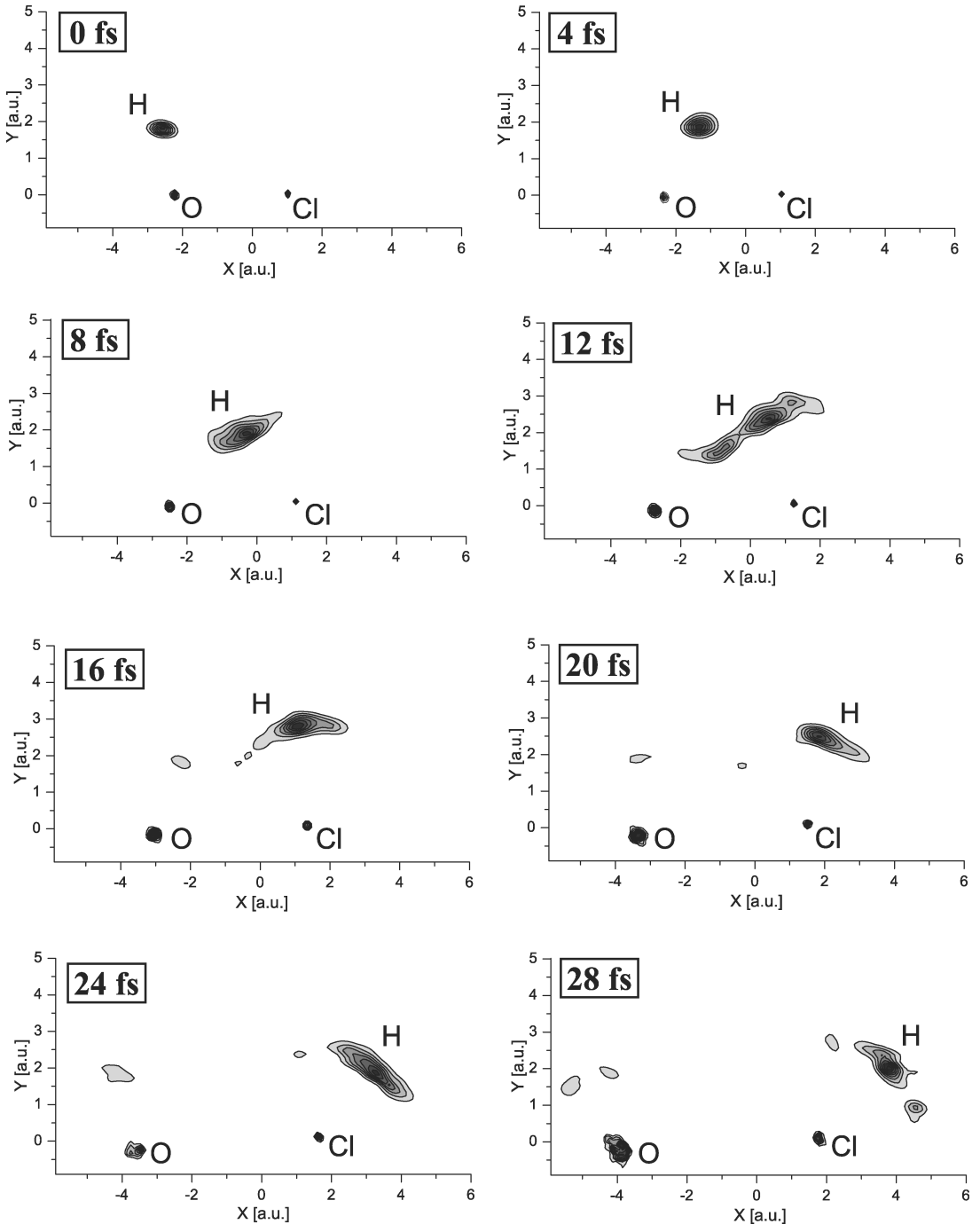

Figure 18. Snapshots of the wave packets of H, O, and Cl at various moments after the electronic excitation of the accelerated ground state wave packet. The *X*-axis is parallel to the initial direction of the O−Cl bond.

by a Gaussian function centered (in atomic units) at $\mathbf{R}_{O=Cl} = (3.2633, 0.0)$ and $\mathbf{R}_H = (-2.5726, 1.7954)$. The width parameters are estimated by fitting the principal modes of the potential wells. The potential energy surfaces of 1A′ and 2A′ states are presented in Figure 16.

To achieve process (i) mentioned above, we set the target state to be a Gaussian wave packet with the same central coordinates and width parameters as those of the initial wave packet, but with the central momenta of hydrogen $\mathbf{P}_H = (16.8, 2.2)$ in atomic units and zero momenta of OCl bond, as illustrated in Figure 16. The target state is designed so that after the almost complete electronic excitation to the 2A′ state the wave packet would start to move toward the OClH configuration. The acceleration is necessary, since on the electronic 2A′ state the HOCl and OClH configurations are separated by a potential barrier. The controlling time for OHCl wave packet acceleration is set to be 900 fs. The final overlap between the controlled wave packet and the target state achieved after 10 iterations is 85%. Figure 17 presents the controlling laser field.

After the wave packet gains the directed momentum, the almost complete electronic excitation to the 2A′ state by quadratically chirped laser pulse is performed. The parameters of the pulse are $\alpha_\omega = 3.3 \times 10^{-5}$ eV/fs^2, $\beta_\omega = 5.17$ eV, and intensity $= 4.25$ TW/cm^2. The resultant wave packet starts to propagate on the excited potential energy surface as shown in Figure 18, where the snapshots are depicted until the final dissociation into the O + HCl channel. The final dissociation

probability is about 92% compared to the almost zero probability in the ordinary photodissociation.

As mentioned at the end of section II.2, the controlling laser field is parallel to the derivative of the dipole moment vector in the direction of the desirable momentum.

V. Concluding Remarks

Laser control of chemical dynamics is not just a simple dream anymore, and now we can challenge a variety of possibilities. Experimental realizations of these ideas may also be expected. Our basic ideas together with their theoretical formulations are presented to control the three elementary processes mentioned in the abstract. Combination of these methods would enable us to effectively control a variety of chemical dynamics.

Numerical demonstrations are presented to show the effectiveness of these methods by taking six-dimensional vibrational photoisomerization of HCN, selective and complete excitation of fine structure levels of K and Cs atoms, photoexcitation and conversion of cyclohexadiene to hexatriene, and photodissociation of OHCl to O + HCl. These numerical examples indicate that the present methods may be applied to various realistic systems. The newly formulated semiclassical *guided* optimal control theory is demonstrated to be able to treat systems of several or more degrees of freedom. Further challenge is needed, of course, to treat much higher dimensions. The quadratic frequency chirping method makes it possible to quickly excite or de-excite multidimensional wave packet with high efficiency close to 100%. Nonadiabatic transitions at conical intersections may be controlled to enhance the desirable transition by giving an appropriate momentum vector to the initial wave packet. This *directed momentum* can be designed by the above-mentioned optimal control theory. In addition to these methods, the intriguing phenomenon of complete reflection that occurs in the nonadiabatic-tunneling-type of potential curve crossing may be utilized to control a certain class of chemical dynamics, although the details of practical applications are not shown here.

As explained in the photoconversion of cyclohexadiene and hexatriene in section IV.2, various molecular functions are governed by nonadiabatic transitions at conical intersections and their overall efficiency including the photoexcitation may actually be controlled by the presently proposed methods. From the viewpoint of nonadiabatic transition, new molecular functions could further be explored and controlled. We believe that this is a prospective and very important subject for the future of molecular science.

Acknowledgment. We thank the support by a Grant-in-Aid for specially Promoted Research on "Studies of Nonadiabatic chemical dynamics based on the Zhu-Nakamura theory" from the MEXT of Japan. Almost all the research reported here were carried out by this support. A.K. also thanks The Ministry of Education of the Russian Federation (DSPHSP2.1.1/4294 and Contract 02.740.11.0447).

References and Notes

(1) Levine, R. D. *Molecular Reaction Dynamics*; Cambridge University Press: Cambridge, U.K., 2005.

(2) Nakamura, H. *J. Phys. Chem.* **2006**, *A110*, 10929.

(3) Brumer, P.; Shapiro, M. *Annu. Rev. Phys. Chem.* **1997**, *48*, 601.

(4) Rice, S. A.; Zhao, M. *Optical Control of Molecular Dynamics*; John Wiley & Sons: New York, 2000.

(5) Nakamura, H. *Nonadiabatic Transition: Concepts, Basic Theories and Applications*; World Scientific: Singapore, 2002.

(6) Bandrauk, A. D.; Fujimura, Y.; Gordon, R. J. *Laser Control and Manipulation of Molecules*; ACS Symposium series 821; American Chemical Society: Washington, DC, 2002.

(7) Brumer, P.; Shapiro, M. *Principles of the Quantum Control of Molecular Processes*; John Wiley & Sons: New York, 2003.

(8) Yamanouchi, K., Chin, S. L., Agostini, P., Ferrante, G., Eds. *Progress in Ultrafast Intense Laser Science*; Springer: Berlin, 2006.

(9) Bonacic-Koutecky, V.; Mitric, R. *Chem. Rev.* **2005**, *105*, 11.

(10) Nakamura, H. *Adv. Chem. Phys.* **2008**, *138*, 95.

(11) Rego, L. G. G.; Santos, L.; Batista, V. S. *Annu. Rev. Chem. Phys.* **2009**, *60*, 293.

(12) Brixner, T.; Gerber, G. *Chem. Phys.* **2003**, *4*, 418.

(13) Wolpert, D.; Schade, M.; Langhojer, F.; Gerber, G.; Brixner, T. *J. Phys. B* **2008**, *41*, 074025.

(14) Bay, T.; Wollenhaupt, M.; Baumert, T. *J. Phys. B* **2008**, *41*, 074007.

(15) Rice, S. A. *Science* **1992**, *258*, 412.

(16) Warren, W. S.; Rabitz, H.; Dahleh, M. *Science* **1993**, *259*, 1581.

(17) Tannor, D.; Rice, S. A. *J. Chem. Phys.* **1985**, *83*, 5013.

(18) Tannor, D. J.; Kosloff, R.; Rice, S. A. *J. Chem. Phys.* **1986**, *85*, 5805.

(19) Kosloff, R.; Rice, S. A.; Gaspard, P.; Tersigni, S.; Tannor, D. *Chem. Phys.* **1989**, *139*, 291.

(20) Sugawara, M.; Fujimura, Y. *J. Chem. Phys.* **1994**, *100*, 5646.

(21) Ohtsuki, Y.; Kono, H.; Fujimura, Y. *J. Chem. Phys.* **1998**, *109*, 9318.

(22) Henriksen, N. E. *Adv. Chem. Phys.* **1995**, *91*, 433.

(23) Kondorskiy, A.; Nakamura, H. *J. Theo. Comput. Chem.* **2005**, *4*, 75. Kondorskiy, A.; Mil'nikov, G.; Nakamura, H. *Phys. Rev.* **2005**, *A72*, 041501.

(24) Kondorskiy, A.; Mil'nikov, G.; Nakamura, H. Progress in Ultrafast Intense Laser Science; Yamanouchi, K., Chin, S. L., Agostini, P., Ferrante, G., Eds.; Springer: Berlin, 2006; Section 6.

(25) Teranishi, Y.; Nakamura, H. *Phys. Rev. Lett.* **1998**, *81*, 2032.

(26) Chelkowski, S.; Bandrauk, A. D.; Corkum, P. B. *Phys. Rev. Lett.* **1990**, *65*, 2355.

(27) Chelkowski, S.; Bandrauk, A. D. *Chem. Chem. Lett.* **1991**, *186*, 264.

(28) Mishima, K.; Yamashita, K. *J. Chem. Phys.* **1998**, *109*, 1801.

(29) Elghobashi, N.; Krause, P.; Manz, J.; Oppel, M. *Phys. Chem. Chem. Phys.* **2003**, *5*, 4806.

(30) Tamura, H.; Nanbu, S.; Ishida, T.; Nakamura, H. *J. Chem. Phys.* **2006**, *124*, 084313.

(31) Zhu, C.; Nakamura, H. *J. Math. Phys.* **1992**, *33*, 2697.

(32) Zhu, C.; Nakamura, H.; Re, N.; Aquilanti, V. *J. Chem. Phys.* **1992**, *97*, 1892.

(33) Zhu, C.; Nakamura, H. *J. Chem. Phys.* **1992**, *97*, 8497; **1993**, *98*, 6208; **1994**, *101*, 4855; **1998**, *108*, 7501; **1994**, *101*, 10630; **1995**, *102*, 7448; **1998**, *109*, 4689; **1997**, *106*, 2599; **1997**, *107*, 7839; *Chem. Phys. Lett.* **1996**, *258*, 342; **1997**, *274*, 205; *Comput. Phys. Commun.* **1993**, *74*, 9.

(34) Nanbu, S.; Ishida, T.; Nakamura, H. *Chem. Phys.* **2006**, *125*, 721.

(35) Shi, S.; Woody, A.; Rabitz, H. *J. Chem. Phys.* **1988**, *88*, 6870.

(36) Schwieters, C. D.; Rabitz, H. *Phys. Rev.* **1993**, *A48*, 2549.

(37) Herman, M. F.; Kluk, E. *J. Chem. Phys.* **1984**, *91*, 27. Kluk, E.; Herman, M. F.; Davis, H. D. *J. Chem. Phys.* **1986**, *84*, 326. Herman, M. F. *Annu. Rev. Phys. Chem.* **1994**, *45*, 83.

(38) Manz, J.; Paramonov, G. K. *J. Phys. Chem.* **1993**, *97*, 12625.

(39) Mitric, R.; Hartmann, M.; Pittner, J.; Bonacic-Koutecky, V. *J. Phys. Chem.* **2002**, *106*, 10477.

(40) Domcke, W.; Yarkony, D.; Köppel, H. *Conical Intersections*; World Scientific: Singapore: 2004.

(41) Magnus, W. *Commun. Pure Appl. Math.* **1954**, *VII*, 649.

(42) Nagaya, K.; Teranishi, Y.; Nakamura, H. *Laser Control and Manipulation of Molecules*; ACS Symposium series 821; American Chemical Society: Washington, DC, 2002; Chapter 7.

(43) Teranishi, Y.; Nakamura, H. *J. Chem. Phys.* **1999**, *111*, 1415.

(44) Zou, S.; Kondorskiy, A.; Mil'nikov, G.; Nakamura, H. *J. Chem. Phys.* **2005**, *122*, 084112.

(45) Zou, S.; Kondorskiy, A.; Mil'nikov, G.; Nakamura, H. In *Progress in Ultrafast Intense Laser Science*; Yamanouchi, K., Chin, S. L., Agostini, P., Ferrante, G., Eds.; Springer: Berlin, 2006; Section 5.

(46) Gaubatz, U.; Rudecki, P.; Schiemann, S.; Bergmann, K. *J. Chem. Phys.* **1990**, *92*, 5363.

(47) Nakamura, H. *J. Chem. Phys.* **1997**, *97*, 256.

(48) Nanbu, S.; Nakamura, H.; Goodman, F. O. *J. Chem. Phys.* **1997**, *107*, 5445.

(49) Nakamura, H. *J. Chem. Phys.* **1999**, *110*, 10253.

(50) Zhang, H.; Smith, S. C.; Nanbu, S.; Nakamura, H. *J. Phys.: Condens. Matter* **2009**, *21*, 144209.

(51) Child, M. *Mol. Phys.* **1976**, *32*, 1495.

(52) Fujisaki, J.; Teranishi, Y.; Nakamura, H. *J. Theo. Comput. Chem.* **2002**, *2*, 245.

(53) Nagaya, K.; Teranishi, Y.; Nakamura, H. *J. Chem. Phys.* **2000**, *113*, 6197.

(54) Pichl, L.; Nakamura, H.; Horacek, J. *J. Chem. Phys.* **2000**, *113*, 906.

(55) Miller, W. H. *J. Phys. Chem.* **2001**, *A105*, 2942. Wang, H.; Sun, X.; Miller, W. H. *J. Chem. Phys.* **1998**, *108*, 9726. Sun, X.; Wang, H.; Miller, W. H. *J. Chem. Phys.* **1998**, *109*, 4190.

(56) Heller, E. *J. Chem. Phys.* **1998**, *94*, 2723.

(57) Walton, A.; Manolopoulos, D. *Mol. Phys.* **1996**, *87*, 961.

(58) Dion, C. M.; Keller, A.; Atabek, O.; Bandrauk, A. D. *Phys. Rev. A* **1999**, *59*, 1382.

(59) Jakubetz, W.; Leong Lan, B. *Chem. Phys.* **1997**, *217*, 375.

(60) Gong, J.; Ma, A.; Rice, S. A. *J. Chem. Phys.* **2005**, *122*, 144311.

(61) Kondorskiy, A.; Milnikov, G.; Nakamura, H. *Phys. Rev. A* **2005**, *72*, 041401(R). Kondorskiy, A.; Nakamura, H. *Phys. Rev. A* **2008**, *77*, 043407.

(62) van Mourik, T.; Harris, G. J.; Polyansky, O. L.; Tennyson, J.; Császár, A. G.; Knowles, P. J. *J. Chem. Phys.* **2001**, *115*, 3706.

(63) Irie, M. *Chem. Rev.* **2000**, *100*, 1685. Irie, M.; Kobatake, S.; Horichi, M. *Science* **2001**, *291*, 1769.

(64) Kompa, K. L.; Levine, R. D. *Proc. Natl. Acad. Sci. U.S.A.* **2001**, *16*, 410.

(65) Murakami, M.; Miyasaka, H.; Okada, T.; Kobatake, S.; Irie, M. *J. Am. Chem. Soc.* **2004**, *126*, 14764.

(66) Tamura, H.; Nanbu, S.; Ishida, T.; Nakamura, H. *J. Chem. Phys.* **2006**, *124*, 084313; **2006**, *125*, 034307.

(67) Fuss, W.; Schmid, W. E.; Trushin, S. A. *J. Chem. Phys.* **2000**, *112*, 8347.

(68) Jacobs, H. J. C.; Havinga, E. *Photochemistry of Vitamin D and Its Isomers and of Simple Trienes*; Pitts, J. N., Hammond, S. G., Gollnick, K., Eds.; Advances in Photochemistry; John Wiley & Sons: New York, 1979; Vol. 11, p 305.

(69) Hoki, K.; Ohtsuki, Y.; Kono, H.; Fujimura, Y. *J. Phys. Chem.* **1999**, *A103*, 6301.

(70) Geppert, D.; Seyfarth, L.; de Vivie-Riedle, R. *Appl. Phys. B: Laser Opt.* **2004**, *79*, 987. de Vivie-Riedle, R.; Hofmann, A. In *Conical Intersections; electronic structure, dynamics and spectroscopy* Domcke, W., Yarkony, D. R., Köppel, H., Eds.; World Scientific: Singapore, 2004.

(71) Geppert, D.; de Vivie-Riedle, R. *Chem. Phys. Lett.* **2005**, *404*, 289.

(72) Hofmann, A.; de Vivie-Riedle, R. *J. Chem. Phys.* **2000**, *112*, 5054; *Chem. Phys. Lett.* **2001**, *346*, 299.

(73) Ramsey, N. F. *Molecular Beams*; Oxford University Press: Oxford, U.K., 1956.

(74) Yamada, H; Yokoyama, K.; Teranishi, A; Sugita, T.; Shirai, T.; Aoyama, Y.; Akahane, N.; Inoue, H.; Ueda, K.; Yamakawa, A.; Yokoyama, A.; Kawaqsaki, H.; Nakamura, H. *Phys. Rev.* **2005**, *A72*, 063404.

(75) Teranishi, Y. *Phys. Rev. Lett.* **2006**, *97*, 053001.

(76) Nanbu, S.; Aoyagi, M.; Kamisaka, H.; Nakamura, H.; Bian, W.; Tanaka, K. *J. Theor. Comput. Chem.* **2002**, *1*, 263; **2002**, *275*, 285.

JP911579H